Acetic acid hydrodeoxygenation on molybdenum carbide catalysts

Journal:	*Catalysis Science & Technology*
Manuscript ID	CY-ART-02-2018-000358.R1
Article Type:	Paper
Date Submitted by the Author:	28-Mar-2018
Complete List of Authors:	Kumar, Anurag; University of Minnesota, Chemical Engineering and Materials Science Phadke, Sohan; University of Minnesota, Chemical Engineering and Materials Science Bhan, Aditya; University of Minnesota, Chemical Engineering and Materials Science

Acetic acid hydrodeoxygenation on molybdenum carbide catalysts

Anurag Kumar, Sohan Phadke, Aditya Bhan*

Department of Chemical Engineering and Materials Science, University of Minnesota-Twin Cities, 421 Washington Avenue SE, Minneapolis, Minnesota 55455, United States

*Corresponding Author: E-mail: abhan@umn.edu; Fax: (+1) 612-626-7246

Abstract

As-synthesized molybdenum carbide shows >98% selectivity (deoxygenated products) and stable chemical conversion for >30 h time-on-stream after an initial deactivation period of ~9 h for vapor phase hydrodeoxygenation of acetic acid at low temperature (403 K) and atmospheric pressure. Space time variation studies show acetaldehyde as a primary unstable product, ethanol as a secondary unstable product, and ethyl acetate and ethylene as secondary stable products suggesting a sequential reaction pathway for acetic acid deoxygenation on Mo_2C. The concurrent half and zero-order dependence of acetic acid HDO rates on H_2 and acetic acid pressure, respectively, suggests that catalytic sites for H_2 activation are distinct from those required for the activation of acetic acid consistent with prior reports for deoxygenation of aromatic ethers and alcohols. Catalyst surface evolution by oxygen ($O:Mo_{bulk} \sim 0.3$) and carbon ($C:Mo_{bulk} \sim 0.1$) deposition from the reactant oxygenate was noted using temperature programmed surface reaction (TPSR) with hydrogen post reaction. Higher O*/Mo deposition with acetic acid in reference to H_2O, CO_2, and aromatic ethers at similar oxygenate pressures suggests that identity of the oxygenate determines its proficiency for heteroatom deposition on fresh carbidic materials. Catalytic site densities were estimated via in-situ titration using 2,2-dimethylpropanoic acid (DMPA) as a reagent to calculate a turnover frequency (TOF) of $(9 \pm 1) \times 10^{-4}$ mol s^{-1} mol_{DMPA}^{-1}. X-ray diffraction patterns and X-ray photoelectron spectra of passivated Mo_2C catalyst samples before and after acetic acid reaction indicate the presence of a carbide/ oxycarbide phase, even though the bulk structure of orthorhombic β-Mo_2C is retained.

1. Introduction

Process chemistries that eliminate oxygen are required for the conversion of biomass to fuels and chemicals. It is desirable that the stoichiometric oxygen removal occur through C-O and/or C=O bond cleavage while keeping C-C bonds intact.[1,2] Pyrolytic methods for biomass decomposition result in bio-oil consisting of corrosive carboxylic acids (~25 wt%) and their derivatives resulting in challenges in downstream processing due to low energy density, high viscosity, and high acid number of the final fuel.[3–5] Deoxygenation of carboxylic acids has been studied predominantly in liquid phase reactions on noble metal catalysts demonstrating complete hydrogenation and low deoxygenation selectivity due to C-C bond scission.[6–10] In contrast, recent reports present non-precious transition metal carbides as stable and selective catalysts for low temperature (~ 433 K) and atmospheric pressure hydrodeoxygenation (HDO) of biomass-derived aromatic ethers[11,12], alcohols[13,14], and aldehydes[15]. Selective catalytic deoxygenation of C_2 oxygenates (acetaldehyde, acetic acid, ethylene glycol, and glycoldehyde) to form ethylene on Mo_2C and WC catalysts was demonstrated using surface science and density functional theory (DFT) studies.[16–19] Acetic acid deoxygenation to acetaldehyde and ethylene on a passivated-reduced Mo_2C catalyst at high temperature (523 – 673 K) and atmospheric pressure was reported by Schaidle et al.[2] Temperature-programmed reaction in conjunction with DRIFTS, XPS, and DFT studies were performed to study the evolution of reaction pathways with increasing temperature.[2] Surface properties of unpassivated as-synthesized Mo_2C were also reported and the catalyst surface was noted to evolve under experimental reaction conditions.[2] C-O bond cleavage was favored at temperatures ranging from 523 – 673 K whereas C-C bond cleavage, via decarbonylation and decarboxylation, was prominent at temperatures ranging from 673 – 773 K.[2] C-O bond cleavage was postulated to occur on acidic

or oxygen vacancy sites and the availability of adsorbed hydrogen from H_2 dissociation was proposed to be rate limiting due to high oxygen surface coverages as inferred in temperature dependent DRIFTS and XPS studies.[2] Here, we report detailed kinetic and mechanistic studies for acetic acid hydrodeoxygenation on as-synthesized molybdenum carbide catalysts at low temperature (~403 K) and atmospheric hydrogen pressure and note distinct site requirements for hydrogen and oxygenate activation.

In-situ structural evolution due to deposition of heteroatoms contributes to the functionality of metal carbides for deoxygenation applications.[20–22] The reactivity of transition metal carbide catalysts is strongly influenced by the adsorption of surface adatoms and by the sub-surface oxygen and carbon content as evinced by surface science studies[23,24], electronic structure calculations[25], and probe reactions [26–29]. WC retains ~50% of oxygen, even after thermal treatment in hydrogen flow at 1150 K, demonstrating the difficulty of complete oxygen removal in metal carbide catalysts.[30] Chemisorbed oxygen on/in tungsten carbide catalyst resulted in the genesis of acidic sites, resulting in increased alkane isomerization rates (with high selectivity of 70 – 99%), while inhibiting the hydrogenolysis rate.[28] In this work, we perform exhaustive temperature programmed surface reaction studies to compare oxygen and carbon deposition from acetic acid on/in as-prepared Mo_2C under reaction conditions in reference to other oxygenates to note the higher efficacy with which acetic acid deposits O-adatoms compared to H_2O, CO_2, and anisole.

The presence of heteroatoms results in metal carbides possessing multiple chemical functions active as catalytic centers as evident from their ability to catalyze hydrogenolysis,[26,31] hydrogenation,[26,32,33] dehydration,[34] and isomerization[35,36] reactions. Temperature programmed desorption (TPD) and probe reaction studies demonstrate the presence of acidic,

basic, and metallic sites on self-supporting Mo_2C catalysts.[34,37] Atmospheric pressure hydrodeoxygenation of anisole leads to in-situ oxidation of molybdenum carbide as evinced through transient kinetic studies and temperature-programmed surface reaction (TPSR) with hydrogen.[38] The highly oxophilic nature of metal carbides and the inevitable structural evolution during hydrodeoxygenation reaction necessitates in-situ characterization of metal carbide catalysts for deoxygenation applications. In this report, we use a site-selective titrant, 2,2 dimethylpropanoic acid (DMPA), for quantification of active sites under reaction conditions.[38–40]

We report as-synthesized molybdenum carbide formulations as stable and selective catalysts for hydrodeoxygenation of acetic acid at 403 K and ambient hydrogen pressure. Mo_2C catalysts selectively cleave the C-O bond in acetic acid to form acetaldehyde, which is subsequently hydrogenated to ethanol, without any C-C bond cleavage (>98% selectivity to acetaldehyde and ethanol). Ethane selectivity was <1 % demonstrating high hydrogen efficiency during catalysis. Rates of acetic acid HDO (1.2×10^{-9} mol s^{-1} g_{cat}^{-1}) were noted to decrease less than 10% over ~48 h time-on-stream after an initial deactivation period, which was attributed to the accumulation of oxygen and carbon as inferred using temperature-programmed surface reaction with hydrogen, consistent with prior reports of self-passivation and carbon deposition on metal carbides.[38,41] Space time studies were performed to demonstrate that acetic acid HDO proceeds via a sequence of deoxygenation-hydrogenation-dehydration-hydrogenation steps and site densities were assessed using in-situ 2,2-dimethylpropanoic acid (DMPA) chemical titration. Plausible reaction schemes involving two distinct sites for hydrogen and acetic acid adsorption are proposed based on detailed kinetic measurements performed in this work. The marked stability and deoxygenation selectivity and the low reaction temperature and low H_2 pressure

employed presents molybdenum carbide as a promising catalyst for catalytic deoxygenation, particularly of bio-oil derived carboxylic acids.

2. Materials and Methods

2.1 Catalyst synthesis

Molybdenum carbide (Mo_2C) catalysts were prepared by a temperature-programmed carburization method reported previously.[11–13,42] Briefly, 0.14 – 1.15 g of the precursor, ammonium molybdate tetrahydrate (AMT, $(NH_4)_6Mo_7O_{24}\cdot 4H_2O$ sieved, 177 − 400 μm, Sigma, 99.98%) was loaded into a tubular quartz reactor with a thermocouple attached to the reactor outer surface (I.D. 4 mm) and purged in a flow of CH_4 (Matheson, 99.97%)/H_2 (Minneapolis Oxygen, 99.999%) (16/84 vol %, total flow rate ~2.97 $cm^3\ s^{-1}$) for ~10 min at room temperature (RT) and then heated in a single-zone split tube furnace (Series 3210, Applied Test System) with a typical temperature protocol as follows. The reactor was heated from RT to ~623 K in 1.5 h, and then held for 5 h. Subsequently, the reactor was heated to ~873 K in 1.5 h and held at the final temperature for 3 h prior to being cooled to the reaction temperature (403 K) or RT in the same CH_4/H_2 gas mixture flow, to begin reaction or passivation, respectively.

The passivated samples for ex-situ characterization were prepared according to the temperature protocol described above. The catalyst was cooled from ~873 K to RT in CH_4/H_2 flow. The Mo_2C catalyst was then treated in a flow of 1% O_2/He mixture (Matheson, Certified Standard Purity) at ~1.67 $cm^3\ s^{-1}$ for 20 – 30 min to passivate the carbidic surface.[11,12] The reactor temperature increased from RT to ~323 K upon the introduction of a 1% O_2/He gas mixture due to the pyrophoric/oxophilic nature of as-synthesized Mo_2C catalysts.[20,44]

2.2 Catalyst characterization

Surface area, porosity, and CO chemisorption capacity of passivated molybdenum carbide samples were determined using an ASAP Micromeritics 2020. Prior to N_2 physisorption measurements, samples were degassed to <6 μm Hg and heated to 523 K at 0.17 K s^{-1} and held for 2 – 4 h.

For CO chemisorption measurements, the sample was evacuated at 383 K (~2 μm Hg) for 0.5 h followed by treatment in H_2 at 723 K for 2 h, and degassed (~2 μm Hg) at 723 K for 2 h. Subsequently, the first CO adsorption isotherm was measured at 323 K. The sample was then degassed (~2 μm Hg) leading to removal of weakly adsorbed CO, followed by a second isotherm measurement. The amount of irreversibly adsorbed CO was obtained from the difference between the two isotherms after extrapolation to zero pressure.[11–13]

The bulk structure of the passivated molybdenum carbide catalysts was characterized using X-ray diffraction (XRD) using a Bruker D8 Discover 2D X-ray diffractometer with a 2-D VÅNTEC-500 detector, Co Kα X-ray radiation with a graphite monochromator, and a 0.5 mm point collimator. Scans were measured in three measurement frames at 30° (2θ), 60° (2θ), and 90° (2θ) at 600 s $frame^{-1}$ while oscillating the sample by 1 mm in both x and y planes. The three 2D scans were converted to 1D intensity vs 2θ plots for analysis and the radiation wavelength was recalibrated for Cu K_α wavelength (λ = 1.541 Å).

A PHI 5000 VersaProbe III (ULVAC-PHI, Inc.) equipped with a monochromated Al K_α X-ray source was used for X-ray photoelectron spectroscopy (XPS) measurements. The base pressure was maintained at 1.0 x 10^{-8} Torr which changed to 5.0 x 10^{-7} Torr during data collection. An approximate area of 1 mm x 1 mm was illuminated with 200W X-rays. The

survey spectra were collected using 280 eV pass energy and 1 eV $step^{-1}$ whereas high-resolution spectra were collected using 50 eV pass energy and 0.1 eV $step^{-1}$. Multipak software provided with the XPS system was used to calculate the atomic percentages from the survey spectrum. All other elements were referenced with respect to the 1s peak of adventitious carbon, set at 285.0 eV. Curve fitting was done using a combination of Gaussian/Lorentzian functions with the Gaussian percentages being at 80% or higher. The Mo $3d_{5/2}$ and $3d_{3/2}$ peaks were fixed with a shift of 3.2 eV for Mo^{6+} and 3.15 eV for both Mo^{4+} and Mo^{3+}. Area ratios of the Mo 3d doublets were optimized so that $A_{5/2}/A_{3/2}$ ~1.5.

2.3 Vapor phase acetic acid HDO kinetic measurements

Rates for vapor-phase acetic acid HDO were measured in a tubular quartz reactor (I.D. 4 mm) with a thermocouple in contact with the reactor outer surface to monitor reaction temperature. Acetic acid (Sigma, 99.99%, Trace metal basis, 0.14 – 6.30 kPa) was fed using a syringe pump (KD Scientific, Model 100) and all flow lines were heated to temperatures in excess of 373 K via resistive heating to prevent condensation of effluents. The composition of the reactor effluent was analyzed using a mass spectrometer (MKS Cirrus 200 Quadrupole MS system) and a gas chromatograph (Agilent 6890) equipped with a methyl-siloxane capillary column (HP-1, 50 m x 320 μm x 0.52 μm) connected to a flame ionization detector (FID). The effluent concentration was quantified using cyclohexane as an internal standard. Cyclohexane did not undergo dehydrogenation or C-C bond cleavage on Mo_2C catalyst at acetic acid HDO reaction conditions reported in this work. Moreover, cyclohexane co-feed during acetic acid HDO did not result in any change in product distribution (data shown in Supporting Information Figure S1).

Once the reactor was cooled to ~403 K from the final synthesis temperature of 873 K, the gas stream was switched from the CH_4/H_2 gas mixture to the reactant mixture (acetic acid/H_2 = 0.14 – 6.30 kPa/balance, total flow rate ~1.67 $cm^3\ s^{-1}$) to perform vapor phase acetic acid hydrodeoxygenation on as-synthesized catalysts without any exposure to oxygen at ambient pressure. The acetic acid conversion and product selectivity are defined as follows:

$$\text{Acetic acid conversion} = \frac{(\text{sum of moles of carbons in products})_{out}}{(\text{moles of carbons in acetic acid})_{in}} \quad (1)$$

$$\text{Selectivity of product i} = \frac{(\text{moles of product i})_{out}}{(\text{sum of moles of products})_{out}} \quad (2)$$

HDO kinetic studies were performed at <10 % acetic acid conversion. Space time studies (0.06 – 26 h $g_{cat}\ g_{acetic\ acid}^{-1}$) were performed by varying the total gas flow rates from 0.33 to 6.17 $cm^3\ s^{-1}$ isobarically at ambient pressure with invariant partial pressures of 1 kPa of acetic acid, 0.07 kPa of cyclohexane, and balance H_2. Proportional variation of all liquid and gas flows at constant catalyst loading as well as independent experiments with different catalyst loadings (to ensure the catalyst bed was isothermal) from 0.095 to 0.72 g were used to achieve the desired variations mentioned above. H_2 (11 – 107 kPa at 0.21 kPa acetic acid and balance argon, total flow rate ~1.67 $cm^3\ s^{-1}$ and catalyst loading = 101 mg) and acetic acid (0.14 – 6.30 kPa at 107 kPa H_2, total flow rate ~1.67 $cm^3\ s^{-1}$ and catalyst loading = 63 mg) partial pressures were varied at constant contact time by altering H_2, inert (Ar), and liquid flow rates. The carbon balance was typically better than 98%, and error associated with quantification for acetic acid and its products was ~5% (calculated from 5 independent measurements of GC response factors).

2.4 In-situ 2,2-dimethylpropanoic acid (DMPA) titrations

In-situ DMPA titration experiments were performed after steady state acetic acid HDO rates were observed. A mixture of liquid DMPA (0.04 – 0.38 kPa) with Ar (~0.03 cm^3 s^{-1}) as inert carrier gas was co-fed in the reactant stream of acetic acid/H_2 with a total flow rate ~1.67 cm^3 s^{-1}. The transient response of Ar and DMPA for each titration experiment was monitored using an online mass spectrometer whereas the product concentration (used to calculate acetic acid HDO rates) was tracked using a gas chromatograph. Argon was used as a tracer to calculate the average residence time of DMPA over the catalyst bed, which was used to determine the amount of DMPA adsorbed on Mo_2C during titration as discussed in Section 3.4. The turnover frequency (TOF) for acetic acid HDO was calculated assuming that one DMPA molecule titrates one active site. Multiple titration experiments at varying DMPA pressures (0.04 – 0.38 kPa) were performed to determine the error associated with TOF calculation.

2.5 Temperature-Programmed Surface Reaction (TPSR) with H_2 after acetic acid HDO

Temperature-programmed surface reaction with H_2 was performed on the Mo_2C catalyst after acetic acid HDO for ~90 ks on-stream at 403 K and atmospheric pressure to quantify the amount of O- and C-adatoms deposited on the catalyst during hydrodeoxygenation. The reactor feed was switched from a mixture of acetic acid/cyclohexane/H_2 to a H_2/Ar gas mixture (81.5/18.5 vol %, total flow rate ~2.6 cm^3 s^{-1}) at 403 K for ~0.6 ks. Subsequently, the sample was heated from 403 K to 723 K at a ramp rate of 0.09 K s^{-1}. The reactor effluent was monitored using a mass spectrometer.

3. Results and Discussion

3.1 Molybdenum carbide catalyst performance for acetic acid HDO

Figure 1 shows the acetic acid conversion and product selectivity for vapor phase acetic acid hydrodeoxygenation on as-synthesized Mo_2C at 403 K and ambient pressure. Acetic acid conversion on Mo_2C catalyst drops by ~40 % over a ~9 hour period initially but is stable for >30 hours after the initial deactivation (Figure 1(a)). Acetaldehyde and ethanol are observed as the major products, accounting for >98 % of the carbon products at ~ 1.4 % acetic acid conversion (Figure 1(b)) at steady state, whereas ethane, ethylene, and ethyl acetate are observed as side products with <2% product selectivity. Acetic acid reaction studies on Pt catalysts at 423 – 573 K, 0.1 – 0.9 atm hydrogen, and 0.009 – 0.065 atm acetic acid feed showed decarbonylation (C-C bond cleavage) as the dominant reaction pathway.[44] In contrast, we report as-synthesized Mo_2C as a selective and stable catalyst for deoxygenation of carboxylic acids at 403 K and atmospheric H_2 pressure.

The initial catalyst deactivation can be attributed to carbon deposition or restructuring of the surface that leads to a loss in the accessibility or number of active sites,[11] and/or formation of an oxycarbide or sub-surface oxygen by oxygen deposition. Acetic acid conversion as well as product selectivity could be fully restored by performing a temperature-programmed surface reaction (TPSR) with hydrogen at 723 K on the spent catalyst demonstrating that the carbon and oxygen deposited on/in the catalyst during reaction can be removed by reaction with hydrogen at high temperature (shown in Figure 2(a) and (b)). Analysis of the reactor effluent during TPSR with hydrogen showed that water and carbon monoxide are the only products observed in the effluent confirming that carbon and oxygen are deposited on/in the catalyst during acetic acid HDO (shown in Figure 2(c)). Quantification of the amount of oxygen retained in the catalyst (considering both H_2O and CO) gave $O:Mo_{bulk}$ ~ 0.30. Lee et al. [38] demonstrated using TPSR

with H_2 and transient kinetic studies that $O:Mo_{bulk} \sim 0.04$ is deposited on molybdenum carbide during anisole hydrodeoxygenation at 423 K. Chen et al.[41] showed oxygen deposition from O_2, H_2O, and CO_2 at 333 K resulted in $O:Mo_{bulk}$ of 0.05 – 0.23 via systematic treatment of as-synthesized Mo_2C with oxidants and TPSR studies. Higher O*/Mo deposition with acetic acid ($O:Mo_{bulk} \sim 0.30$) at similar oxygenate pressures (0.75 – 1 kPa) demonstrates that carboxylic acids are more potent oxidants as compared to aromatic ethers, H_2O ($O:Mo_{bulk} \sim 0.038$), or CO_2 ($O:Mo_{bulk} \sim 0.035$) but comparable to O_2 ($O:Mo_{bulk} \sim 0.23$). Liu et al. [45] performed DFT calculations on C-terminated and Mo-terminated Mo_2C to show that a Mo oxycarbide can be formed during water gas shift on Mo_2C surfaces due to chemisorbed oxygen from water dissociation. Prasomsri et al.[46] concluded that MoO_3 can be partially carburized during HDO to generate oxycarbide or oxycarbohydride phases as evinced by XPS (observation of Mo^{5+} species) and XRD (observation of oxycarbohydride phase). Shi et al.[47] performed DFT calculations to show that O_2 adsorbs dissociatively and exothermically on low-index surfaces, including pure or oxygen-covered β-Mo_2C(100) and β-Mo_2C(011) surfaces with strongly negative adsorption energies (~ -3 eV at 0 K). Our results in conjunction with these studies demonstrate that heteroatom deposition and site density and identity for metal carbide catalysts during reactions of oxygen-containing molecules are likely a strong function of the reactant used.

In-situ oxidation of Mo_2C by anisole during catalysis has been shown to suppress the hydrogenation functionality of the catalyst leading to reduced cyclohexane selectivity from anisole HDO and resulting in benzene being the predominant stable aromatic product. [38] The stable and selective nature of Mo_2C for acetic acid deoxygenation with low selectivity for the hydrogenation product, ethane, can similarly be attributed to the deposition of O-adatoms by acetic acid. Oyama and co-workers [48] performed TPSR with H_2 on molybdenum carbides

prepared using different carburization conditions to identify three types of carbonaceous species, near surface carbide, polymeric, and graphitic carbon, on Mo_2C, demonstrating the susceptibility of metal carbides for depositing carbonaceous species. The amount of carbon evolved during TPSR (based on CO, the only carbon containing product observed in the effluent as shown in Figure 2(c)) was calculated to be $C:Mo_{bulk} \sim 0.1$ which suggests that carbonaceous species are retained in the catalyst during acetic acid HDO. A TPSR with hydrogen at 723 K on as-synthesized Mo_2C without acetic acid exposure did not yield any carbon containing molecules in the effluent, suggesting that the carbon in CO evolved during hydrogen TPSR of Mo_2C post-acetic acid reaction is a result of carbon deposited from acetic acid during deoxygenation. Lee et al. [38] reported that $C:Mo_{bulk} \sim 0.17$ eluted from passivated-activated Mo_2C formulations during TPSR following anisole hydrodeoxygenation at 423 K and 1 atm. Lu et al.[49] reported a cumulative accumulation of ~0.1 monolayer of C_1 over 54 ks time-on-stream during anisole hydrodeoxygenation on mesoporous Mo_2C at 423 K. These results in conjunction with our TPSR experiments demonstrate that carbon deposition on carbide catalysts occurs during HDO irrespective of the identity of the oxygenate. Schaidle et al.[2] performed XPS measurements on Mo_2C catalysts after exposure to acetic acid and hydrogen at 623 K for different periods (5 -120 min) to investigate the deposition of oxygen and carbon on the catalyst surface as the reaction progressed. The $O/Mo_{surface}$ atomic ratio (~0.80) was observed to be invariant with increasing time of exposure but the $C/Mo_{surface}$ ratio was noted to increase from 0.80 at 5 min exposure time to 1.34 at 2 h exposure time evincing adventitious carbon deposition from acetic acid. Kinetic measurements reported in this study are not corrupted by transients in time and reflect the Mo_2C catalyst surface functionality after oxygen and carbon accumulation during vapor-phase acetic acid HDO.

3.2 Acetic acid HDO reaction pathways

Results from contact time variation studies performed for acetic acid hydrodeoxygenation are shown in Figure 3. A non-zero initial slope of acetaldehyde partial pressure with contact time, shown in Figure 3(b), confirms acetaldehyde as a primary product. Near-zero initial slopes of product partial pressures with contact time are observed for ethanol, ethylene, ethane, and ethyl acetate (the esterification product from acetic acid and ethanol), as shown in Figures 3(b) and (c), demonstrating that these are either secondary or tertiary products. The rank and stability of each product can be identified by the trend of its selectivity as a function of acetic acid conversion (Figure S2).[50–52] Acetaldehyde is identified as a primary unstable product with continuously decreasing selectivity from an initial non-zero value, indicating that it is formed directly from acetic acid and reacts to generate other products as the reaction progresses. Ethanol is seen as a secondary unstable product with selectivity that attains a maximum from an initial zero. Ethyl acetate and ethylene appear as secondary stable products in our studies with continuously increasing selectivity from initial zero values, suggesting their formation only from other products. We propose a sequential deoxygenation-hydrogenation-dehydration-hydrogenation acetic acid HDO reaction pathway wherein acetic acid is deoxygenated to form acetaldehyde, followed by hydrogenation to form ethanol, which further dehydrates to ethylene and successively hydrogenates to ethane as represented in Scheme 1. Contact time variation experiments were used to show that acetone and propanal deoxygenate via a sequential hydrogenation-dehydration-hydrogenation pathway on both passivated and activated Mo_2C proceeding through equilibrated hydrogenation of acetone to isopropanol, dehydration of isopropyl alcohol to propylene, and subsequently propene hydrogenation to propane at 369 K and 483 K implying that pathways involving deoxygenation-hydrogenation reaction sequences

are typical for atmospheric pressure vapor-phase HDO of molecules containing carbonyl groups over Mo_2C catalysts.[37,42] A direct C=O hydrogenolysis HDO pathway for propanal was proposed over activated Mo_2C and WC catalysts by Chen and co-workers.[15,53] Hydrodeoxygenation of propanal was modeled over clean Mo_2C (0001) surface using density functional theory (DFT) and temperature-programmed desorption (TPD) under ultrahigh-vacuum (UHV) conditions to propose propylene as the primary product with CO, CO_2, H_2O being absent during TPD.[15] Nevertheless, the strong O* binding energy (-5.4 – -8.15 eV)[45] on clean Mo_2C surfaces and the observed in-situ oxidation of Mo_2C catalysts suggests that metal carbides during reactions at ambient pressure and after O* exposure behave differently from as synthesized carbides studied in UHV and using DFT.[42]

Deoxygenation of long chain fatty acids at elevated hydrogen pressures (5 – 50 bar) and reaction temperatures (323 – 633 K) in the liquid phase occurs via a deoxygenation-hydrogenation-dehydration pathway on metal carbide based catalysts as evidenced by the sequential appearance of corresponding aldehydes, alcohols, and alkenes.[1–12] These reports are in line with our proposed deoxygenation-hydrogenation-dehydration-hydrogenation reaction pathway for vapor phase acetic acid HDO on as-synthesized molybdenum carbide catalyst at 403 K and atmospheric hydrogen pressure suggesting that such pathways are typical for hydrodeoxygenation on transition metal carbide catalysts.

Zero selectivity for ethanol at low acetic acid conversion (Figure S2) demonstrates the absence of a direct ethanol formation pathway suggesting that the rate of acetic acid HDO can be calculated as the sum of the rates of formation of acetaldehyde, ethanol, ethylene, and ethane as shown in equation 3.

$$r_{\text{acetic acid HDO}} = r_{f_{\text{acetaldehyde}}} + r_{f_{\text{ethanol}}} + r_{f_{\text{ethylene}}} + r_{f_{\text{ethane}}} \quad (3),$$

where, r_{f_i} = rate of formation of product i

Schaidle et al.[2] noted absence of oxygenate conversion at temperatures below 523 K in independent acetic acid and ethanol temperature-programmed reaction (TPRxn) experiments on passivated-activated Mo_2C at a H_2:acetic acid molar ratio of 3.9 presumably due to the low H_2 feed pressure (H_2:acetic acid ~110 in this study). Acetic acid was observed to form acetaldehyde and ethylene in the temperature range 523 – 673 K via hydrogenation-dehydration pathways, whereas decarbonylation and decarboxylation products CH_4, CO, CO_2 were dominant at temperatures ranging from 673 – 773 K. At temperatures greater than 823 K, CO and H_2, gasification products of acetic acid were predominantly formed. All experimental studies reported herein are at reaction conditions (403 K and atmospheric H_2 pressure) under which deoxygenation of acetic acid to acetaldehyde and ethanol is dominant and C-C bond scission chemistries are almost entirely absent.

The hydrogenation of acetaldehyde to ethanol was always far from equilibrium, even at acetic acid conversion exceeding 40%, as confirmed by an assessment of approach to equilibrium, η, (1.9×10^{-4} – 0.0265) under all acetic acid contact times studied here (0.2 – 26 g_{cat} $g_{\text{acetic acid}}^{-1}$ h; detailed calculation discussed in Supporting Information Section S.3). Metal carbides are known to possess noble-metal-like hydrogenation catalytic functionality.[64–67] Sullivan et al.[42] demonstrated that in-situ oxygen modification of activated Mo_2C catalysts, via 13.5 kPa O_2 co-feed at a reaction temperature of 369 K, decreased the catalyst surface area from 68 to 9 m^2 g^{-1} as measured by post-reaction nitrogen adsorption measurements, and suppressed C=O hydrogenation of acetone to isopropanol but increased acidic dehydration rates by

increasing the Brønsted acid site density. Similar effects of oxygen-modification have been observed for alkane isomerization over WC_x catalysts.[27,68] Schaidle et al.[2] also propose that acetaldehyde hydrogenation to ethanol during acetic acid reactions on passivated-reduced Mo_2C is not thermodynamically limited at 573 K. They observe an approach to equilibrium, η, of 0.012 at 573 K. Hydrogenation was proposed to be slower than C-O bond cleavage on Mo_2C by the authors and they ascribed this to the low concentration of H-adsorption sites. Alternatively, this observation can be related to the low H_2 feed pressure used in their study. The non-equilibrated hydrogenation of acetaldehyde reported here, in conjunction with in-situ oxidation of the catalyst surface discussed in Section 3.1, demonstrates that catalyst passivation by molecules/species with faculty for O* deposition comparable to that of molecular O_2 results in suppressed hydrogenation functionality of metal carbides.

3.3 Acetic acid HDO kinetics and mechanism

Kinetic measurements were performed under steady state reaction conditions (following a ~24 h catalyst deactivation as discussed in Section 3.1). Absence of any heat or mass transfer limitations was affirmed through calculations (presented in Section S.4 of the Supporting Information). Acetic acid HDO was found to be catalytic over molybdenum carbide catalysts as evinced by an estimated turnover number of ~7 after 28 h on-stream (using a surface area of 100 $m^2\ g_{cat}^{-1}$ and a Mo site density of 1 x 10^{15} sites cm^{-2}). Under differential acetic acid conversions (<5%), ethyl acetate selectivity was always <0.2 mole % of the products formed and acetic acid HDO rates could be calculated using Equation (3) as the sum of rates of formation of acetaldehyde, ethanol, ethylene, and ethane.

Figures 4 shows H_2, acetic acid, and water partial pressure dependence of acetic acid HDO rates over molybdenum carbide catalysts. Acetic acid HDO rates were independent of

acetic acid partial pressure (0.14 – 6.30 kPa), as shown in Figure 4(a), indicating that the catalyst surface is saturated by oxygen-containing species similar to earlier reports of anisole, m-cresol, and acetone HDO on molybdenum carbide.[11–13,42] Schaidle et al.[2] performed DFT studies on Mo-Mo_2C(001) and C-Mo_2C(001) surfaces at varying temperature (523 – 873 K), 10.2 kPa hydrogen pressure, and water pressure (0.01 – 10.2 kPa) based on an assessment of phase diagrams using thermodynamic considerations relating the chemical potential to temperature and gas phase composition, to obtain energetically favorable surface oxygen coverage at conditions representative for acetic acid HDO in their study. The results demonstrated an oxygen-saturated surface of molybdenum carbide (0.5 – 1 monolayer oxygen-coverage) attributed to the propensity of metal carbides to strongly adsorb the oxygenate-derived H_2O during acetic acid deoxygenation reaction. DFT studies by Likith et al.[69] for typical water-gas shift and steam methane reforming reaction conditions (473 – 923 K and 0.1 – 0.4 bar oxygenate partial pressure) on Mo-terminated orthorhombic Mo_2C noted that molybdenum oxycarbides ($(Mo_2C)_xO_y$) are formed as stable surface phases at these conditions because carbon and oxygen deposition (0 – 1 monolayer) occurs, also suggesting that oxygenate coverage is high during reactions of oxygen-containing species on metal carbides.

A concurrent half-order dependence of acetic acid HDO rates on hydrogen partial pressure (11 kPa – 107 kPa) at constant acetic acid pressure (0.21 kPa), shown in Fig 4(a), suggests dissociative adsorption of H_2 on sites distinct from acetic acid adsorption sites because if competition between acetic acid and molecular hydrogen existed for same site, we would expect inhibition of HDO rates by acetic acid. A two-site model involving distinct sites for adsorption of acetic acid and hydrogen is consistent with earlier reports of anisole and m-cresol HDO on molybdenum carbide catalysts.[11,12,70] Shi et al.[47,71] calculated the reaction energy of

surface oxidation of $Mo_2C(101)$ and $Mo_2C(011)$ surfaces by O_2 and noted energy differences as large as ~2 eV between $Mo_2C(101)$ and $Mo_2C(011)$. These surfaces differ because C atom incorporation in half of the octahedral interstitial sites distorts hexagonal lattice symmetry and the differences in O_2 adsorption energy between these surfaces suggest that Mo_2C surfaces possess a multitude of adsorption-sites. Jiao and co-workers[33,72–75] performed density functional theory calculations on Mo-terminated as well as mixed Mo/C-terminated carbide surfaces to reveal that the binding energy of CO on hexagonal Mo_2C is lower on the (101) surface relative to (201) and (001) surfaces with adsorption energy differences of ~1.05 eV at saturation CO coverages. Furthermore, H_2 was shown to adsorb dissociatively on on-top, bridging, or hollow sites on (001), (101), and (201) surfaces with adsorption energy differences as high as ~0.20 eV across surfaces. The preferential adsorption of CO and H_2 on on-top, bridging, or hollow sites with changing temperature, pressure, gas phase composition, and surface coverages is consistent with our results suggesting that active centers with varying surface-termination and binding energies exist on β-Mo_2C surfaces which plausibly results in oxygenates adsorbing on sites distinct from metal-like H-adsorption sites.

Acetic acid HDO rates were independent of water partial pressure (0 – 46 Pa, shown in Figure 4(b)), relevant to the reaction conditions studied in this work. Moreover, acetic acid HDO rates were invariant with acetic acid conversion (0.57 – 8.27%) (Supporting Information Section S.7) demonstrating that HDO products do not have any measurable kinetic effects on acetic acid deoxygenation to acetaldehyde, plausibly due to a higher propensity of acetic acid to deposit oxygen as compared to H_2O as discussed in Section 3.1. These results are consistent with absence of product inhibition reported for hydrodeoxygenation of anisole[11], m-cresol[41], acetone[42], and isopropanol[39] over molybdenum carbide catalyst formulations. The apparent

activation energy for acetic acid deoxygenation to acetaldehyde was found to be 67.5 ± 1.5 kJ mol^{-1} as shown in Figure 5.

Figure 6(a) shows that the hydrogen order was independent of the acetic acid partial pressure (0.1 – 0.96 kPa), in line with the two-site model involving distinct sites for hydrogen and acetic acid activation discussed in Section 1 above. As shown in Figure 6(b), the apparent activation energy for acetic acid to acetaldehyde conversion was invariant with acetic acid partial pressure (0.1 – 0.93 kPa), confirming that the catalyst surface is saturated with oxygenate-derived species, even at low concentrations of acetic acid, and that the reaction pathways do not change with feed oxygenate concentration.

We propose two plausible reaction schemes for acetic acid deoxygenation to acetaldehyde (Scheme 2) consistent with the observed rate dependence of ~0.5 order in hydrogen, zero order in acetic acid, and absence of product inhibition. In Scheme 1, H_2 dissociatively adsorbs on site S_1 whereas acetic acid, CH_3COOH, adsorbs on site S_2. The scheme involves formation of an $RC(OH)(OH)\text{-}S_2$ intermediate which undergoes C-O bond cleavage to form an adsorbed acetaldehyde species. Considering (i) addition of dissociated hydrogen to the adsorbed acetic acid intermediate as the rate limiting step, (ii) all other steps to be quasi-equilibrated, and (iii) the most abundant reactive intermediate (MARI) for S_1 to be empty sites and for S_2 to be the adsorbed acetic acid intermediate, we get a rate equation consistent with the experimental observations (detailed derivation in Supporting Information Section S.5.1). Alternatively, in Scheme 2, the oxophilic carbidic surface can strip the oxygen from acetic acid and the resulting intermediate ($RCO\text{-}S_2$) reacts with dissociated hydrogen to form an adsorbed acetaldehyde species. Again, considering (i) the rate determining step to be the addition of dissociated hydrogen to the acetic acid derived intermediate ($RCO\text{-}S_2$), and (ii) empty sites and

RCO-S_2 are MARI for S_1 and S_2 respectively, we can derive a rate equation consistent with the experimental observations (detailed steps in Supporting Information Section S.5.2). These proposals are in line with the reaction schemes postulated for vapor phase furfural hydrodeoxygenation to 2-methylfuran over Mo_2C catalysts at 423 K.[70,76]

3.4 Site density for acetic acid HDO on Mo_2C catalysts

The catalytic site density for acetic acid hydrodeoxygenation on molybdenum carbide catalysts was measured using in-situ 2,2-dimethylpropanoic acid (DMPA) titrations. Acetic acid HDO rates were allowed to reach steady state before a DMPA-Ar mixture was co-fed. Acetic acid HDO rates were found to be suppressed by ~50% in the presence of DMPA, but could be fully restored upon the removal of DMPA (Figure 7), suggesting that DMPA is a reversible titrant. Numerous DMPA titration experiments with varying DMPA partial pressures (0.04 – 0.38 kPa) were performed to calculate the acetic acid HDO turnover frequency (TOF), defined as the sum of the rates of formation of acetaldehyde, ethanol, ethylene, and ethane (Equation 3) per time per DMPA titration site.

Figure 8 shows the normalized reactor effluent signals acquired using an online mass spectrometer, for DMPA and argon during a typical DMPA titration experiment. A blank reactor experiment, where a DMPA-Ar (~1.8 x 10^{-5} cm^3 s^{-1}/~0.06 cm^3 s^{-1}) mixture was co-fed into a reactant flow of acetic acid/H_2 ~0.50 kPa/balance (total flow rate ~1.67 cm^3 s^{-1}) at 403 K and atmospheric pressure, gave a synchronic breakthrough curve for both Ar and DMPA mass spectrometer signals as shown in Figure 8(a). In contrast, a DMPA-Ar co-feed during acetic acid HDO resulted in a delayed breakthrough time for DMPA as compared to the inert tracer Ar (shown in Figure 8(b)) and this apparent residence time of DMPA in the reactor was attributed to adsorption or reaction of DMPA on the Mo_2C catalyst surface.

The number of active catalytic sites occupied by DMPA during titration was calculated as the product of the known DMPA flow rate and the DMPA residence time, which was obtained using two methods. The DMPA residence time can be estimated as the difference in the breakthrough times of DMPA and Ar signals, shown as t_1 in Figure 8(b) and Table 1. This calculation assumes that the DMPA reaction contributes negligibly to the observed DMPA residence time. As shown in Table 1, the amount of DMPA converted to its deoxygenated product during the course of titration (calculated as the product of titration time, t_1 and the DMPA product rate obtained from analysis of gas composition) accounted for <3.5% of the total DMPA adsorbed during titration in all the titration experiments. Alternatively, the average DMPA residence time can be estimated using the area between the Ar and DMPA curves (shown as t_2 in Figure 8(b) and Table 1) after normalizing both signals to their corresponding steady state values.[38] The residence times of DMPA obtained from the two methods discussed above were found to be typically in good agreement (with <15% difference between the two values), as shown in Table 1. The titration experiments at low DMPA liquid flow rates (experiments 4, 11, and 12 in Table 1; 0.009 – 0.017 $cm^3\ h^{-1}$) had greater disparity between the residence times from the two methods due to the instability of liquid feed at extremely low flow rates.

The turnover frequency (TOF) of acetic acid HDO per DMPA titration site on Mo_2C can be calculated on the basis of the ratio of the reduction of acetic acid HDO rate due to the presence of DMPA (Figure 7) and the amount of DMPA adsorbed on the catalyst (as discussed above). This TOF calculation considers (i) one DMPA molecule to poison one active site, and (ii) all active sites to be identical. The acetic acid HDO turnover frequency (TOF) was found to be $9 \pm 1 \times 10^{-4}$ mol s^{-1} mol_{DMPA}^{-1} (Table 1). Similar site densities have been reported using in-

situ CO titration for anisole HDO (TOF ~ 1.1 ± 0.3 × 10^{-3} s^{-1})[38] and m-cresol HDO (TOF ~ 3.6 ± 0.7 × 10^{-3} mol mol_{CO}^{-1} s^{-1})[41] at 423 K over passivated-activated Mo_2C catalysts.

The acetic acid HDO TOF values were found to be nearly invariant with DMPA partial pressure (0.04 – 0.4 kPa; Figure 9 and Figure S3, using breakthrough time t_1 and average residence time t_2, respectively) demonstrating (i) the absence of DMPA mass transfer limitations during in-situ titration, (ii) a negligible effect of DMPA deoxygenation on the TOF calculation, and (iii) little or no diversity in the active sites titrated by DMPA under reaction conditions used in this work.

3.5 Catalyst synthesis and characterization

The molybdenum carbide catalyst was synthesized using procedures described in Section 2.1. X-ray diffraction patterns of passivated catalyst samples before and after acetic acid HDO reaction are shown in Figure 10(a). Catalyst samples both before and after the reaction exhibit primarily the orthorhombic β-Mo_2C phase with a small fraction of metastable FCC α-Mo_2C phase as shown in Figure 10(a). Absence of any peaks assigned to the molybdenum oxide crystalline phases suggests that bulk carburization was achieved. Absence of bulk MoO_2 (2θ = 25°)[39], MoO_3 (2θ = 26°)[39], or MoO_xC_y (2θ = 43° and 15°) [36] phases, even after exposure to atmosphere before XRD measurements, indicates that passivation and acetic acid HDO does not change the bulk structure of Mo_2C crystallites.

XPS analysis of the passivated molybdenum carbide sample before reaction (Figure 10(b)) shows that the surface state comprises of 14.8% Mo^{6+}, 14.8% Mo^{5+}, 26% Mo^{4+}, and 44.3% Mo^{3+}, with Mo $3d_{5/2}$ peaks centered at 232.6, 230.8, 229.6, and 228.9 eV, respectively. Similar XPS analysis of the catalyst sample post acetic acid HDO reaction (Figure 10(c)) showed

that the surface comprised of 8.3% Mo^{6+}, 7.3% Mo^{5+}, 23.5% Mo^{4+}, and 61% Mo^{3+}, with Mo $3d_{5/2}$ peaks centered at 232.2, 230.7, 229.4, and 228.7 eV, respectively. C 1s and O 1s spectra are provided in Supporting Information Section S.8. Handbook of X-ray Photoelectron Spectroscopy[77] was used for standard binding energies of Mo^{6+}, Mo^{4+} and Mo^{5+} assigned at 232.6 eV, 229.2 eV and 231 eV respectively. 228.9 eV was assigned to Mo^{3+} based on reports by Choi et al.[78] and Sullivan et al.[39]. Román-Leshkov and co-workers[46,79] performed XPS studies on spent MoO_3 after hydrodeoxygenation of m-cresol at 573 – 673 K to track the changes in molybdenum oxidation states with increasing reaction temperature. Mo^{5+} (Mo $3d_{5/2}$ peak at 230.8 eV assigned to an oxycarbide phase[80]) accounted for 54 % to 31 % molybdenum on spent MoO_3 demonstrating formation of an oxycarbide during reaction. Also, the amount of Mo^{4+} increased with increasing reaction temperature due to the reduction of Mo^{6+} during reaction. Schaidle et al.[2] performed XPS measurements on Mo_2C catalysts after passivation, H_2 treatment at 673 K, and acetic acid reaction without exposure to atmosphere. Passivated Mo_2C (without atmospheric exposure) showed mostly MoO_3 (Mo^{6+} peak at 232.9 eV) with only 19% Mo_2C (Mo^{2+} peak at 228.4 eV) demonstrating that passivation oxidized the near surface region of as-synthesized Mo_2C to predominantly an oxide.[2] Activation of passivated Mo_2C in H_2 at 673 K results in ~36% Mo^{2+} but mostly higher oxidation states of Mo (Mo^{3+} at 231.3 eV, Mo^{4+} at 229.9 eV and Mo^{5+} at 228.9 eV) assigned to an oxycarbidic phase.[2] O 1s peaks at 532.5 eV (assigned to strongly bound O^-, OH^-, H_2O and O=C) and 531.2 eV (oxygen in oxycarbide or oxy-carbohydride phase) are also observed in both passivated and reduced Mo_2C samples further demonstrating the formation of an oxycarbidic phase on oxygen exposure.[2] XPS after exposure to acetic acid and hydrogen at 623 K for different periods demonstrated that surface hydroxyls and an oxycarbide phase persisted under reaction conditions.[2] The absence of a peak assigned to

Mo^{2+} species in our studies can be attributed to exposure of the sample to the ambient environment prior to XPS analysis. We hypothesize that the as-synthesized Mo_2C used in our reaction studies would only consist of the carbidic phase but the possibility of catalyst evolution into an oxycarbidic phase with reaction progress cannot be excluded. The presence of highly oxidized Mo $3d_{5/2}$ peaks and absence of a peak assigned to Mo_2C (Mo^{2+} state) support our TPSR and kinetic study results that (i) oxygen and carbon deposition from acetic acid feed takes place on as-synthesized Mo_2C catalyst during HDO, and (ii) the catalyst surface is saturated with feed oxygenate. The results above demonstrate (i) the utility of metal carbides for selective deoxygenation of carboxylic acids, (ii) the evolution of the catalyst surface during reaction as evident from post-reaction TPSR studies and a comparison reveals acetic acid as a more potent oxidant than H_2O, CO_2, and anisole for as-synthesized Mo_2C, and (iii) a half order kinetic dependence of HDO rates on H_2 pressure and zero order dependence in oxygenate pressure on molybdenum carbide similar to that observed for aldehydes and aromatic ethers.

4. Conclusions

Molybdenum carbide can catalyze acetic acid hydrodeoxygenation via a sequential deoxygenation-hydrogenation-dehydration-hydrogenation pathway as evidenced by contact time studies. Initial catalyst deactivation is observed for ~24 hours due to accumulation of $O:Mo_{bulk} \sim 0.3$ and $C:Mo_{bulk} \sim 0.1$ of oxygen and carbon, respectively, from the oxygenate reactant, before steady state conversion and rates are achieved. Acetic acid deoxygenation to acetaldehyde occurs through a two-site mechanism involving distinct sites for hydrogen and acetic acid activation.

The products of acetic acid HDO showed no measureable kinetic inhibition effects on HDO rates. Acetic acid HDO does not change the bulk structure of the molybdenum carbide but the presence of an oxycarbidic or oxidic phase on the catalyst surface cannot be ruled out. The acetic acid HDO TOF estimated by in-situ DMPA titration was found to be $9 \pm 1 \times 10^{-4}$ mol s^{-1} mol_{DMPA}^{-1} with an assumption that one DMPA molecule titrates one active site for acetic acid deoxygenation to acetaldehyde.

Acknowledgements

This research was supported by National Science Foundation Catalysis and Biocatalysis Program (CBET Award No. 1510661). Parts of this work were carried out in the Characterization Facility, University of Minnesota, which receives partial support from NSF through the MRSEC program. We thank Ms. Seema Thakral for assistance with the XRD analysis and Bing Luo for XPS measurements.

Notes

The authors declare no competing financial interest.

References

[1] A. Dutta, J. A. Schaidle, D. Humbird, F. G. Baddour, A. Sahir, *Top. Catal.* **2016**, *59*, 2–18.

[2] J. A. Schaidle, J. Blackburn, C. A. Farberow, C. Nash, K. X. Steirer, J. Clark, D. J. Robichaud, D. A. Ruddy, *ACS Catal.* **2016**, *6*, 1181–1197.

[3] G. W. Huber, A. Corma, *Angew. Chem. Int. Ed. Engl.* **2007**, *46*, 7184–201.

[4] S. Dutta, S. De, B. Saha, M. I. Alam, *Catal. Sci. Technol.* **2012**, *2*, 2025–2036.

[5] Marcel Schlaf, Z. Conrad Zhang, *Reaction Pathways and Mechanisms in Thermocatalytic Biomass Conversion I*, **2016**.

[6] G. J. S. Dawes, E. L. Scott, J. Le Nôtre, J. P. M. Sanders, J. H. Bitter, *Green Chem.* **2015**,

17, 3231–3250.

[7] R. W. Gosselink, S. A. W. Hollak, S.-W. Chang, J. van Haveren, K. P. de Jong, J. H. Bitter, D. S. van Es, *ChemSusChem* **2013**, *6*, 1576–94.

[8] D. S. Pankaj Kumar, Sudhakara Reddy Yenumala, Sunil K. Maity, P. Kumar, S. R. Yenumala, S. K. Maity, D. Shee, *Appl. Catal. A Gen.* **2014**, *471*, 28–38.

[9] H. Bernas, E. Kari, S. Irina, A.-R. Leino, K. Kordás, M. Jukka, M.-A. Päivi, T. Salmi, D. Y. Murzin, *Fuel* **2010**, *89*, 2033–2039.

[10] P. Mäki-Arvela, M. Snare, E. Kari, Myllyoja Jukka, D. Y. Murzin, *Fuel* **2008**, *87*, 3543–3549.

[11] W.-S. Lee, Z. Wang, R. J. Wu, A. Bhan, *J. Catal.* **2014**, *319*, 44–53.

[12] C. J. Chen, W. S. Lee, A. Bhan, *Appl. Catal. A Gen.* **2016**, *510*, 42–48.

[13] M. M. Sullivan, A. Bhan, *J. Catal.* **2016**, *344*, 53–58.

[14] S. Boullosa-Eiras, R. Lødeng, H. Bergem, M. Stöcker, L. Hannevold, E. A. Blekkan, *Catal. Today* **2014**, *223*, 44–53.

[15] H. Ren, W. Yu, M. Salciccioli, Y. Chen, Y. Huang, K. Xiong, D. G. Vlachos, J. G. Chen, *ChemSusChem* **2013**, *6*, 798–801.

[16] N. Dubuc, P. H. McBreen, *Top. Catal.* **2015**, *58*, 232–239.

[17] W. Yu, Z. J. Mellinger, M. A. Barteau, J. G. Chen, *J. Phys. Chem. C* **2012**, *116*, 5720–5729.

[18] K. Xiong, W. Yu, J. G. Chen, *Appl. Surf. Sci.* **2014**, *323*, 88–95.

[19] W. Yu, M. A. Barteau, J. G. Chen, *J. Am. Chem. Soc.* **2011**, *133*, 20528–20535.

[20] S. T. Oyama, *Catal. Today* **1992**, *15*, 179–200.

[21] J.-S. Choi, G. Bugli, G. Djéga-Mariadassou, *J. Catal.* **2000**, *193*, 238–247.

[22] K. Xiong, W. Yu, D. G. Vlachos, J. G. Chen, *ChemCatChem* **2015**, *7*, 1402–1421.

[23] E. I. Ko, R. J. Madix, *Surf. Sci.* **1981**, *112*, 373–385.

[24] E. I. Ko, R. J. Madix, *Surf. Sci.* **1980**, *100*, L449–L453.

[25] A. J. Medford, A. Vojvodic, F. Studt, F. Abild-Pedersen, J. K. Nørskov, *J. Catal.* **2012**, *290*, 108–117.

[26] G. S. Ranhotra, A. T. Bell, J. A. Reimer, *J. Catal.* **1987**, *108*, 40–49.

[27] E. Iglesia, J. E. Baumgartner, F. H. Ribeiro, M. Boudart, *J. Catal.* **1991**, *544*, 523–544.

[28] E. Iglesia, F. H. Ribeiro, M. Boudart, J. E. Baumgartner, *Catal. Today* **1992**, *15*, 307–337.

[29] F. H. Ribeiro, R. A. Dalla Betta, M. Boudart, J. E. Baumgartner, E. Iglesia, *J. Catal.* **1991**, *130*, 86–105.

[30] F. H. Ribeiro, R. A. Dalla Betta, G. J. Guskey, M. Boudart, *Chem. Mater.* **1991**, *3*, 805–812.

[31] J. H. Sinfelt, D. J. C. Yates, *Nature* **1971**, *229*, 27–28.

[32] N. N. Nassar, A. Hassan, P. Pereira-Almao, *Energy & Fuels* **2011**, *25*, 3961–3965.

[33] T. Wang, Q. Luo, Y.-W. Li, J. Wang, M. Beller, H. Jiao, *Appl. Catal. A Gen.* **2014**, *478*, 146–156.

[34] S. K. Bej, C. A. Bennett, L. T. Thompson, *Appl. Catal. A Gen.* **2003**, *250*, 197–208.

[35] M. K. Neylon, S. Choi, H. Kwon, K. E. Curry, L. T. Thompson, *Appl. Catal. A Gen.* **1999**, *183*, 253–263.

[36] C. Bouchy, C. Pham-Huu, B. Heinrich, C. Chaumont, M. J. Ledoux, *J. Catal.* **2000**, *190*, 92–103.

[37] S. K. Bej, L. T. Thompson, *Appl. Catal. A Gen.* **2004**, *264*, 141–150.

[38] W.-S. Lee, A. Kumar, Z. Wang, A. Bhan, *ACS Catal.* **2015**, *2*, 4104–4114.

[39] M. M. Sullivan, J. T. Held, A. Bhan, *J. Catal.* **2015**, *326*, 82–91.

[40] J. F. DeWilde, H. Chiang, D. A. Hickman, C. R. Ho, A. Bhan, *ACS Catal.* **2013**, *3*, 798–807.

[41] C. J. Chen, A. Bhan, *ACS Catal.* **2017**, *7*, 1113–1122.

[42] M. M. Sullivan, A. Bhan, *ACS Catal.* **2016**, *6*, 1145–1152.

[43] U. L. Pasteur, *Catal. Today* **1996**, *27*, 145–150.

[44] W. Rachmady, M. A. Vannice, *J. Catal.* **2000**, *192*, 322–334.

[45] P. Liu, J. A. Rodriguez, *J. Phys. Chem. B* **2006**, *110*, 19418–19425.

[46] T. Prasomsri, M. Shetty, K. Murugappan, Y. Román-Leshkov, *Energy Environ. Sci.* **2014**, *7*, 2660–2669.

[47] X.-R. Shi, S.-G. Wang, J. Wang, *J. Mol. Catal. A Chem.* **2016**, *417*, 53–63.

[48] T. Miyao, I. Shishikura, M. Matsuoka, M. Nagai, S. T. Oyama, *Appl. Catal. A Gen.* **1997**, *165*, 419–428.

[49] Q. Lu, C.-J. Chen, W. Luc, J. G. Chen, A. Bhan, F. Jiao, *ACS Catal.* **2016**, *6*, 3506–3514.

[50] N. A. Bhore, M. T. Klein, K. B. Bischoff, *Chem. Eng. Sci.* **1990**, *45*, 2109–2116.

[51] N. A. Bhore, M. T. Klein, K. B. Bischoff, *Ind. Eng. Chem. Res.* **1990**, *29*, 313–316.

[52] L. Bui, A. Bhan, *Appl. Catal. A Gen.* **2017**, *546*, 87–95.

[53] H. Ren, Y. Chen, Y. Huang, W. Deng, D. G. Vlachos, J. G. Chen, *Green Chem.* **2014**, *16*, 761–769.

[54] R. W. Gosselink, D. R. Stellwagen, J. H. Bitter, *Angew. Chemie* **2013**, *125*, 5089–5092.

[55] E. Santillan-Jimenez, M. Crocker, *J. Chem. Technol. Biotechnol.* **2012**, *87*, 1041–1050.

[56] A. Enferadi Kerenkan, F. Béland, T.-O. Do, *Catal. Sci. Technol.* **2016**, *6*, 971–987.

[57] A. S. Rocha, L. A. Souza, R. R. Oliveira, A. B. Rocha, V. Teixeira da Silva, *Appl. Catal. A Gen.* **2017**, *531*, 69–78.

[58] M. A. Patel, M. A. S. Baldanza, V. T. Da Silva, A. V. Bridgwater, *Appl. Catal. A Gen.* **2013**, *458*, 48–54.

[59] J. Quiroz, E. F. Mai, V. Teixeira da Silva, *Top. Catal.* **2016**, *59*, 148–158.

[60] B. Rozmyszowicz, M.-A. Paivi, A. Tokarev, A.-R. Leino, K. Eranen, D. Yu Murzin, *Ind. Eng. Chem. Res* **2012**, *51*, 8922–8927.

[61] S. A. W. Hollak, R. W. Gosselink, D. S. van Es, J. H. Bitter, *ACS Catal.* **2013**, *3*, 2837–2844.

[62] D. R. Stellwagen, J. H. Bitter, *Green Chem.* **2015**, *17*, 582–593.

[63] L. Souza Macedo, D. R. Stellwagen, V. Teixeira da Silva, J. H. Bitter, *ChemCatChem* **2015**, *7*, 2816–2823.

[64] A. S. Rocha, A. B. Rocha, V. T. da Silva, *Appl. Catal. A Gen.* **2010**, *379*, 54–60.

[65] J. S. Lee, M. H. Yeom, K. Y. Park, I.-S. Nam, J. S. Chung, Y. G. Kim, S. H. Moon, *J. Catal.* **1991**, *128*, 126–136.

[66] J. S. Choi, J. M. Krafft, A. Krzton, G. Djéga-Mariadassou, *Catal. Letters* **2002**, *81*, 175–180.

[67] R. R. Oliveira, A. S. Rocha, V. Teixeira da Silva, A. B. Rocha, *Appl. Catal. A Gen.* **2014**, *469*, 139–145.

[68] V. Keller, P. Wehrer, F. Garin, R. Ducros, G. Maire, *J. Catal.* **1995**, *153*, 9–16.

[69] S. R. J. Likith, C. A. Farberow, S. Manna, A. Abdulslam, V. Stevanović, D. A. Ruddy, J. A. Schaidle, D. J. Robichaud, C. V. Ciobanu, *J. Phys. Chem. C* **2018**, *122*, 1223–1233.

[70] W.-S. Lee, Z. Wang, W. Zheng, D. G. Vlachos, A. Bhan, *Catal. Sci. Technol.* **2014**, *4*, 2340–2352.

[71] X.-R. Shi, S.-G. Wang, J. Hu, Z. Qin, J. Wang, *Surf. Sci.* **2012**, *606*, 1187–1194.

[72] T. Wang, Y.-W. Li, J. Wang, M. Beller, H. Jiao, *J. Phys. Chem. C* **2014**, *118*, 8079–8089.

[73] T. Wang, S. Wang, Y.-W. Li, J. Wang, H. Jiao, *J. Phys. Chem. C* **2012**, *116*, 6340–6348.

[74] T. Wang, Y.-W. Li, J. Wang, M. Beller, H. Jiao, *J. Phys. Chem. C* **2014**, *118*, 3162–3171.

[75] M. M. Sullivan, C.-J. Chen, A. Bhan, *Catal. Sci. Technol.* **2016**, *6*, 602–616.

[76] K. Xiong, W.-S. Lee, A. Bhan, J. G. Chen, *ChemSusChem* **2014**, *7*, 2146–2151.

[77] J. F. Moulder, J. Chastain, *Handbook of X-Ray Photoelectron Spectroscopy : A Reference Book of Standard Spectra for Identification and Interpretation of XPS Data*, Physical

Electronics Division, Perkin-Elmer Corp, **1992**.

[78] J. G. Choi, L. T. Thompson, *Appl. Surf. Sci.* **1996**, *93*, 143–149.

[79] T. Prasomsri, T. Nimmanwudipong, Y. Román-Leshkov, *Energy Environ. Sci.* **2013**, *6*, 1732–1738.

[80] P. Delporte, F. Meunier, C. Pham-Huu, P. Vennegues, M. J. Ledoux, J. Guille, *Catal. Today* **1995**, *23*, 251–267.

Figures and Tables

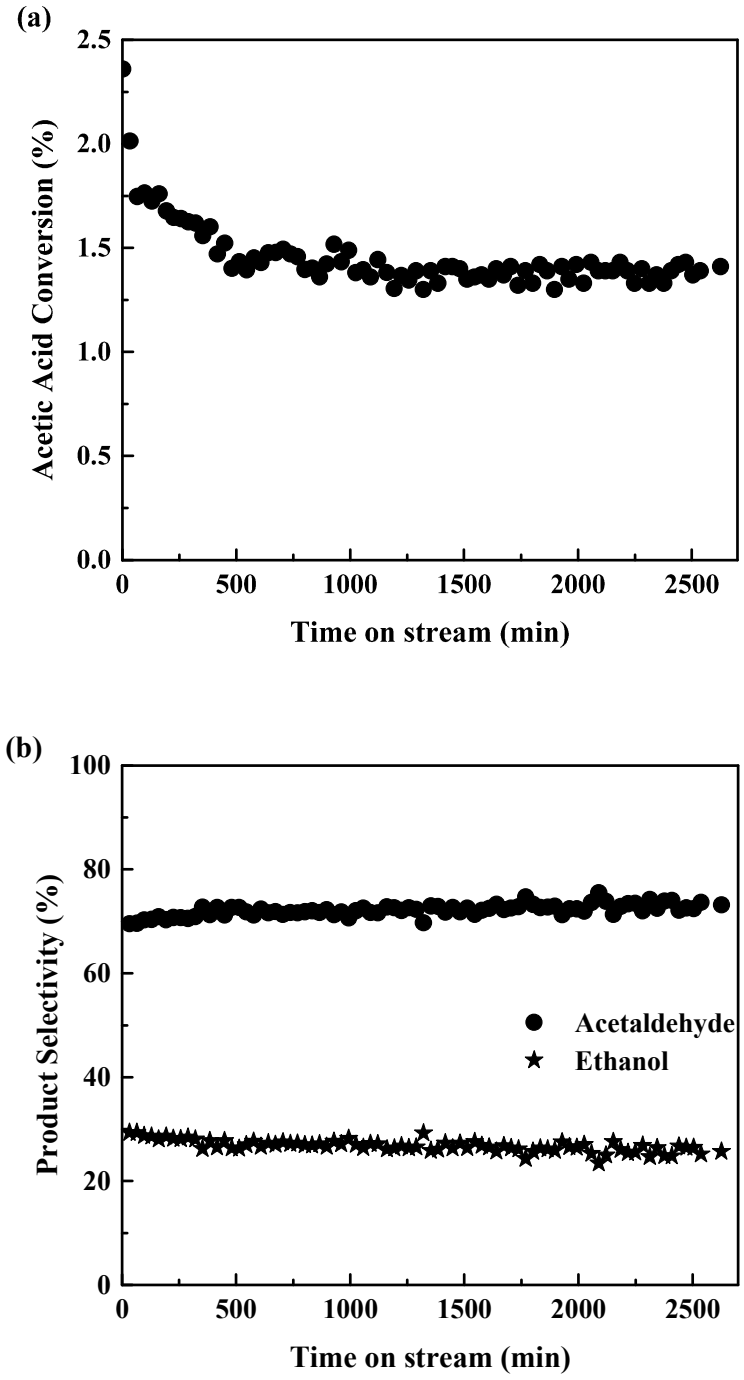

Figure 1. (a) Acetic acid conversion and (b) measured product selectivity of acetaldehyde and ethanol as a function of time-on-stream at 403 K and 1 atm. Reaction conditions: acetic acid/ cyclohexane/ H_2 = 1.5 kPa/0.07 kPa/balance, total flow rate ~1.67 cm^3 s^{-1} and catalyst loading = 88 mg.

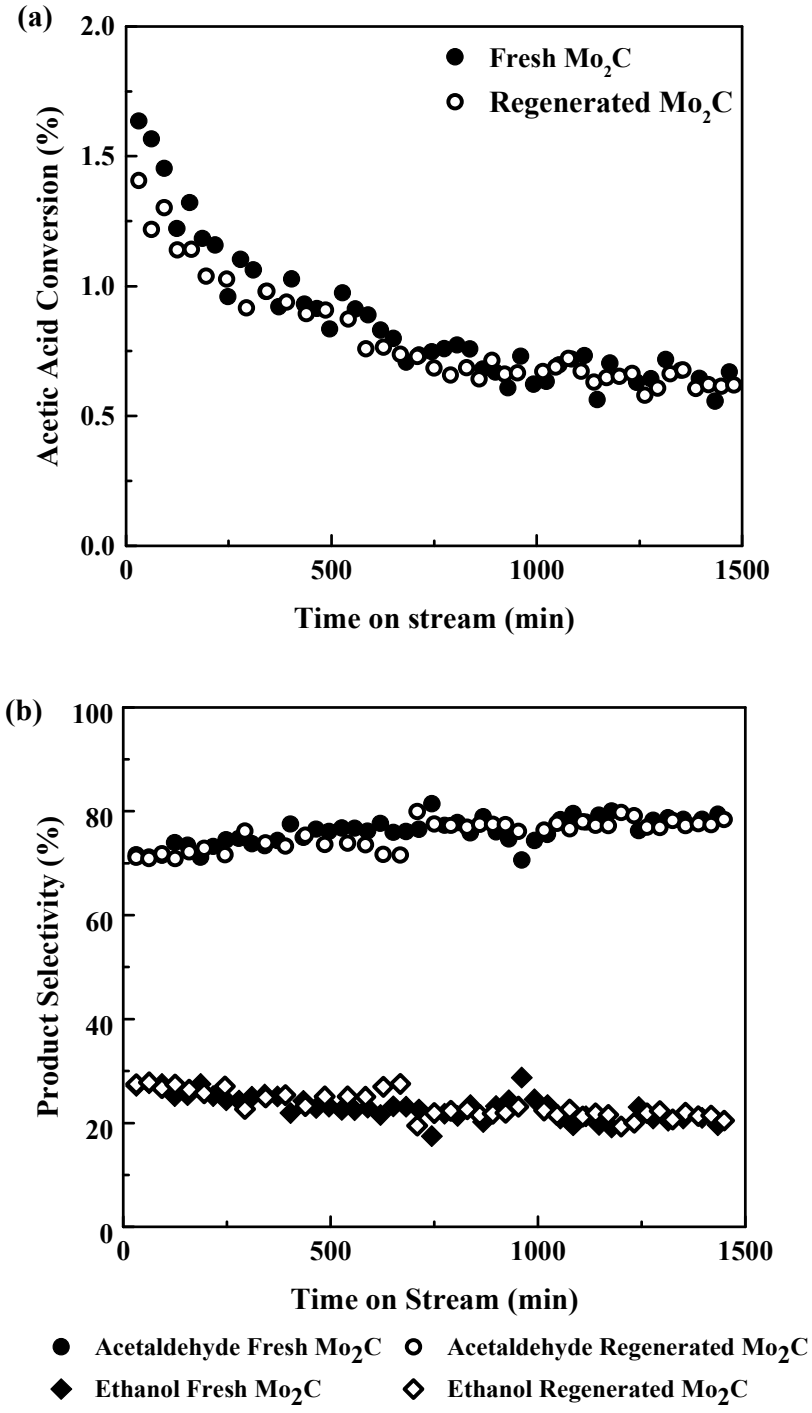
(a)
Fresh Mo_2C
Regenerated Mo_2C
Acetic Acid Conversion (%)
Time on stream (min)
(b)
Product Selectivity (%)
Time on Stream (min)
Acetaldehyde Fresh Mo_2C
Acetaldehyde Regenerated Mo_2C
Ethanol Fresh Mo_2C
Ethanol Regenerated Mo_2C

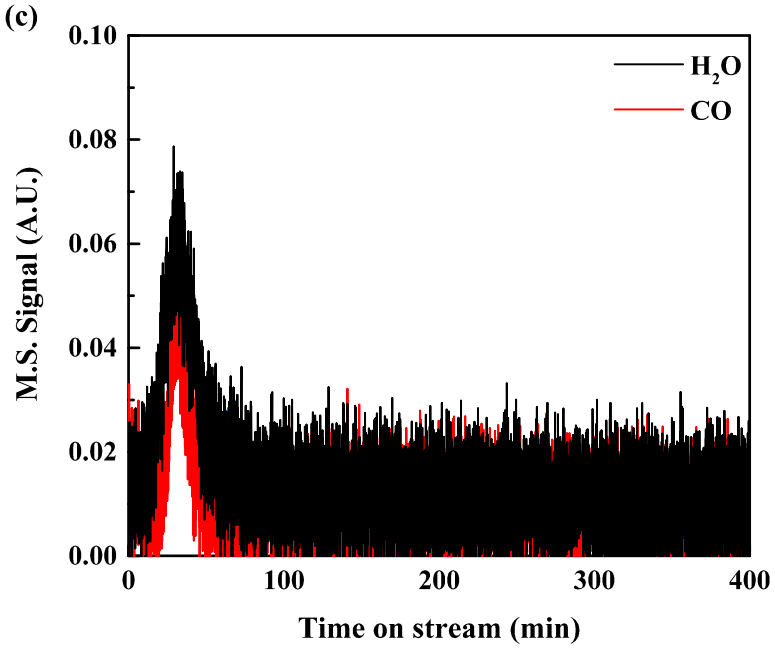

Figure 2. (a) Acetic acid conversion and (b) measured product selectivity of acetaldehyde and ethanol as a function of time-on-stream at 403 K and 1 atm. Fresh Mo_2C catalyst (black data points) and the same catalyst after regeneration (red data points). Reaction conditions: acetic acid/ cyclohexane/ H_2 = 1 kPa/0.07 kPa/balance, total flow rate ~1.67 cm^3 s^{-1} and catalyst loading = 83 mg. (c) Temperature-programmed surface reaction with H_2 (TPSR) of the Mo_2C catalyst after vapor phase acetic acid HDO for ~1500 minutes shown in Figure 2(a) and (b). The catalyst was purged in a flow of H_2/Ar (81.5/18.5 vol %, total flow rate ~2.6 cm^3 s^{-1}) at ~403 K for ~10 minutes; subsequently, the temperature was ramped from ~403 K to ~723 K with a ramp rate ~0.09 K s^{-1}.

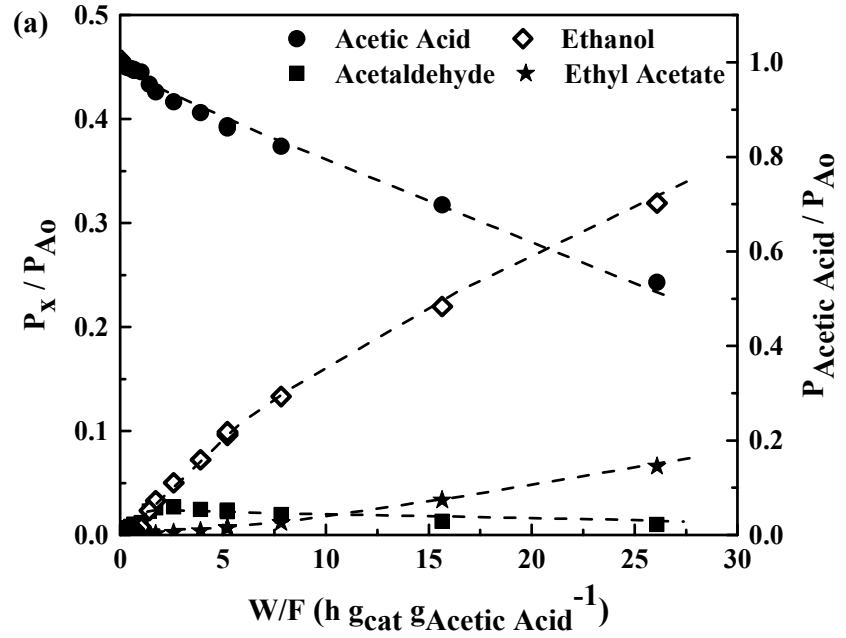
(a)
Acetic Acid
Ethanol
Acetaldehyde
Ethyl Acetate
P_X / P_{Ao}
$P_{Acetic\ Acid} / P_{Ao}$
W/F (h g_{cat} $g_{Acetic\ Acid}^{-1}$)

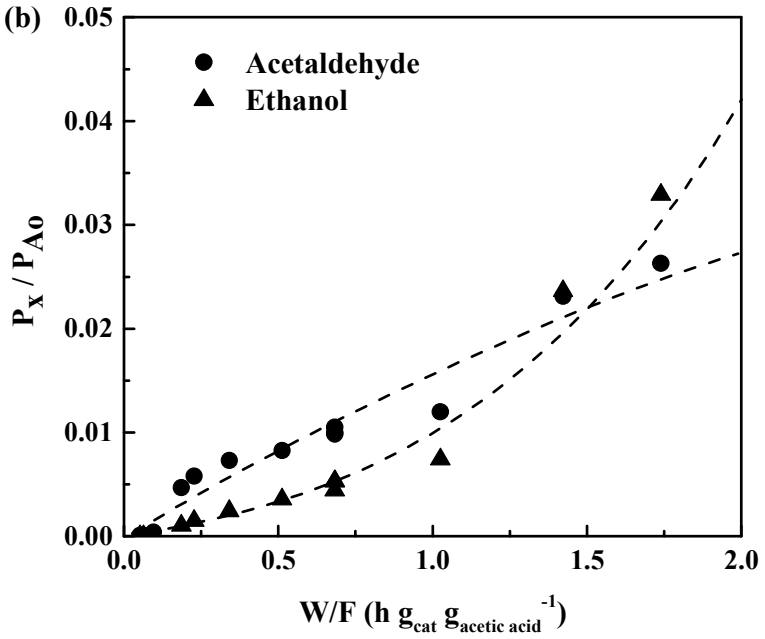
(b)
Acetaldehyde
Ethanol
P_X / P_{Ao}
W/F (h g_{cat} $g_{acetic\ acid}^{-1}$)

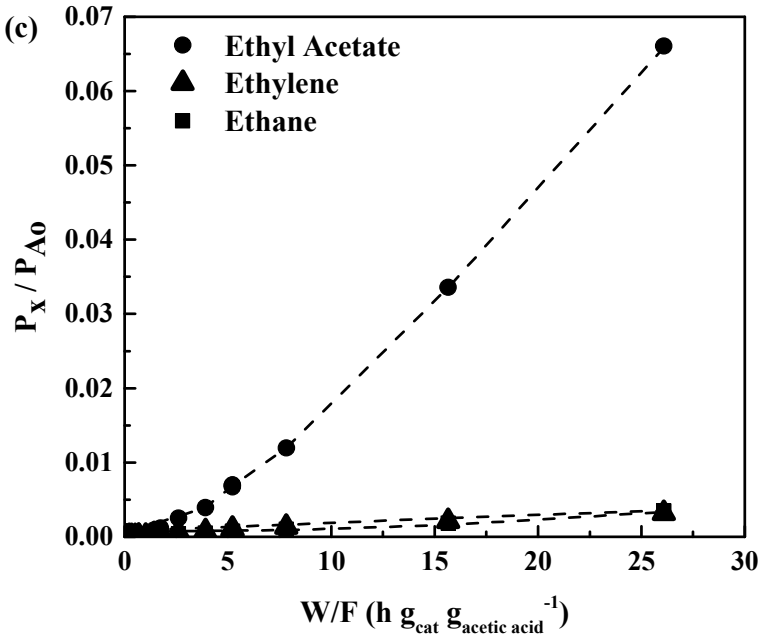

Figure 3. (a) Normalized effluent partial pressures as a function of contact time (0.06 – 26 h g_{cat} $g_{acetic\ acid}^{-1}$). (b) Normalized effluent partial pressures for major products at short contact times (0.06 – 1.73 h g_{cat} $g_{acetic\ acid}^{-1}$). (c) Normalized effluent partial pressures as a function of contact time (0.06 – 26 h g_{cat} $g_{acetic\ acid}^{-1}$) for side products in acetic acid HDO. Reaction conditions: temperature = 403 K, pressure = 1 atm, acetic acid/ cyclohexane/ H_2 = 1 kPa/0.07 kPa/balance, total flow rate was varied from 0.33 – 6.17 cm^3 s^{-1} and catalyst loading was 95 mg and 720 mg in two independent experiments. Acetic acid conversion varied from 0.008 % to 46 %. Dashed lines are included as a guide to the eye.

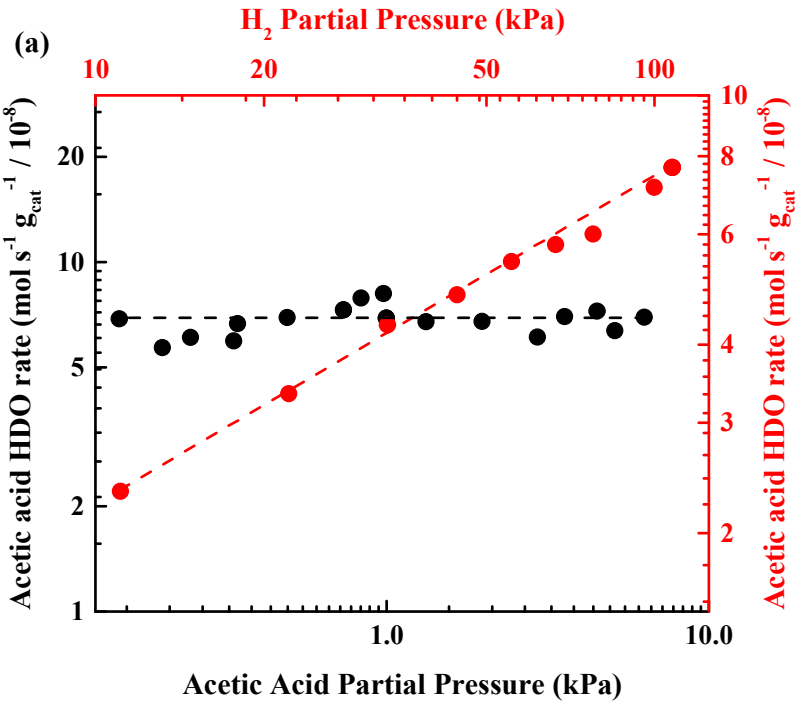

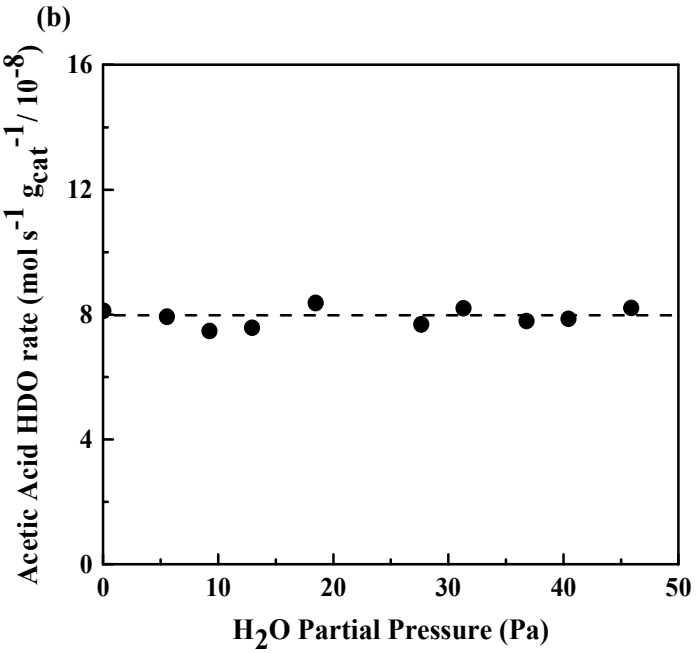

Figure 4. (a) Effect of H_2 partial pressure (red data points, varied from 11 – 107 kPa at 0.21 kPa acetic acid and balance argon, total flow rate ~1.67 cm^3 s^{-1}, temperature = 403 K and catalyst loading = 101 mg) and acetic acid partial pressure (black data points, varied from 0.14 – 6.30 kPa at 107 kPa H_2, total flow rate ~1.67 cm^3 s^{-1}, temperature = 403 K and catalyst loading = 63 mg). (b) Effect of water partial pressure (varied from 0 – 46 Pa at 1 kPa acetic acid and 106 kPa H_2, total flow rate ~1.67 cm^3 s^{-1}, temperature = 403 K and catalyst loading = 90 mg). Acetic acid conversion was in the range 0.75 – 4.40 %. Dashed lines are included as a guide to the eye.

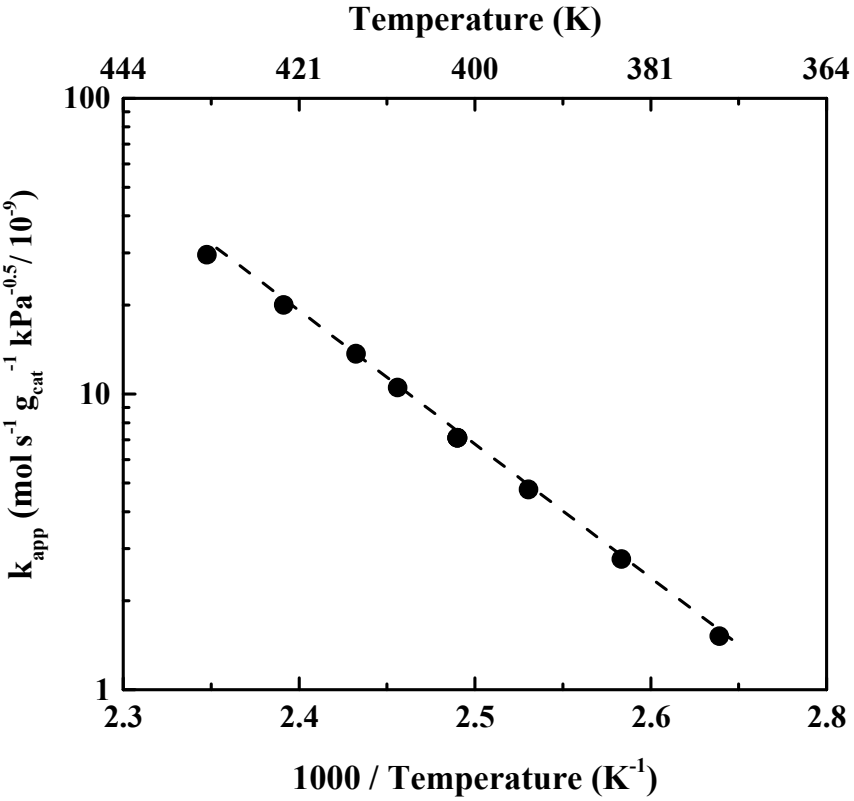

Figure 5. Logarithmic plot of k_{app} (= acetic acid HDO rate/$P_{H_2}^{0.5}$) vs inverse temperature. Reaction conditions: temperature varied from 373 – 433 K at acetic acid/ cyclohexane/ H_2 = 0.2 kPa/0.32 kPa/balance, total flow rate ~1.67 cm^3 s^{-1} and catalyst loading = 88 mg. Acetic acid conversion in the range 1.1 – 4.5 %.

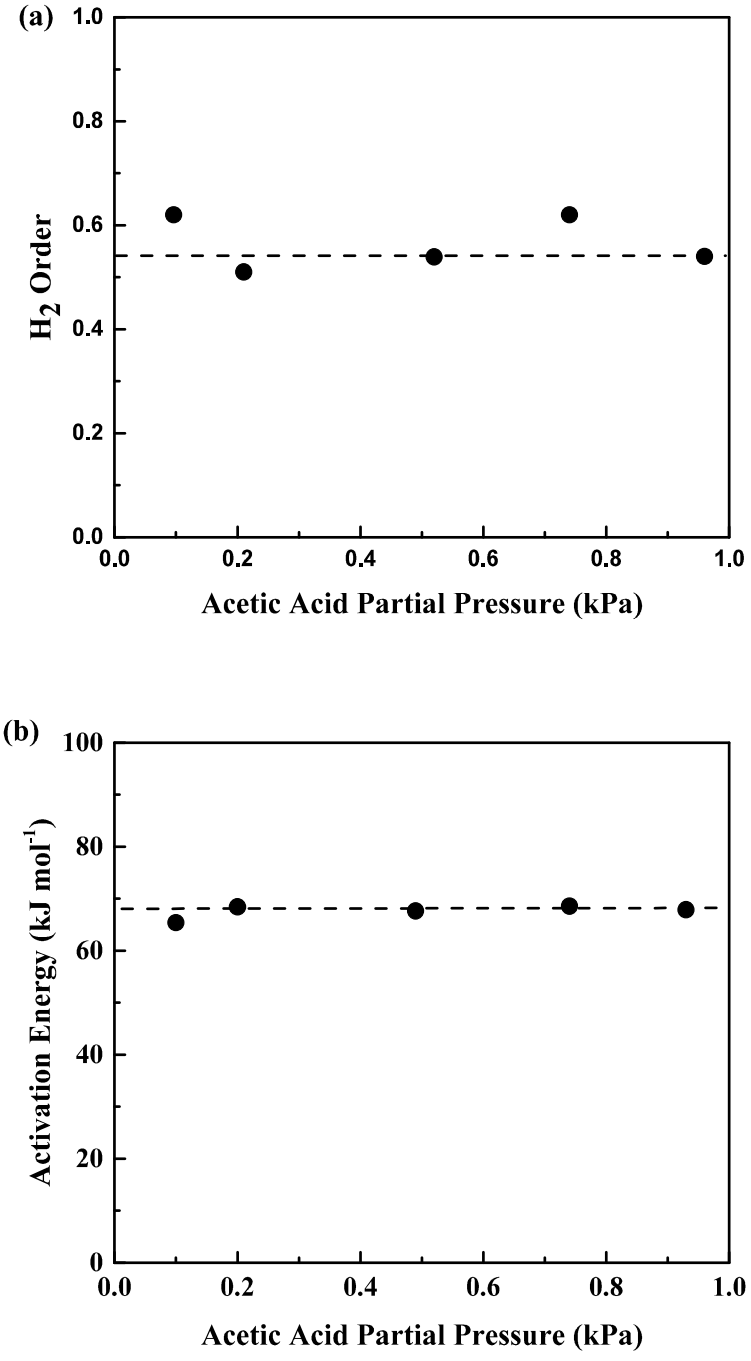

Figure 6. (a) H_2 order and (b) apparent activation energy as a function of acetic acid partial pressure. Reaction conditions: For (a), H_2 partial pressure varied from 11 – 107 kPa at 0.10 – 0.96

kPa acetic acid pressure and balance argon, total flow rate ~1.67 cm^3 s^{-1}, temperature = 403 K and catalyst loading = 101 mg. For (b), temperature varied from 373 – 433 K at 0.10 – 0.96 kPa acetic acid pressure/ 0.32 kPa cyclohexane/ balance H_2, total flow rate ~1.67 cm^3 s^{-1} and catalyst loading = 88 mg. Acetic acid conversion ranged from 0.2 – 7.0 %.

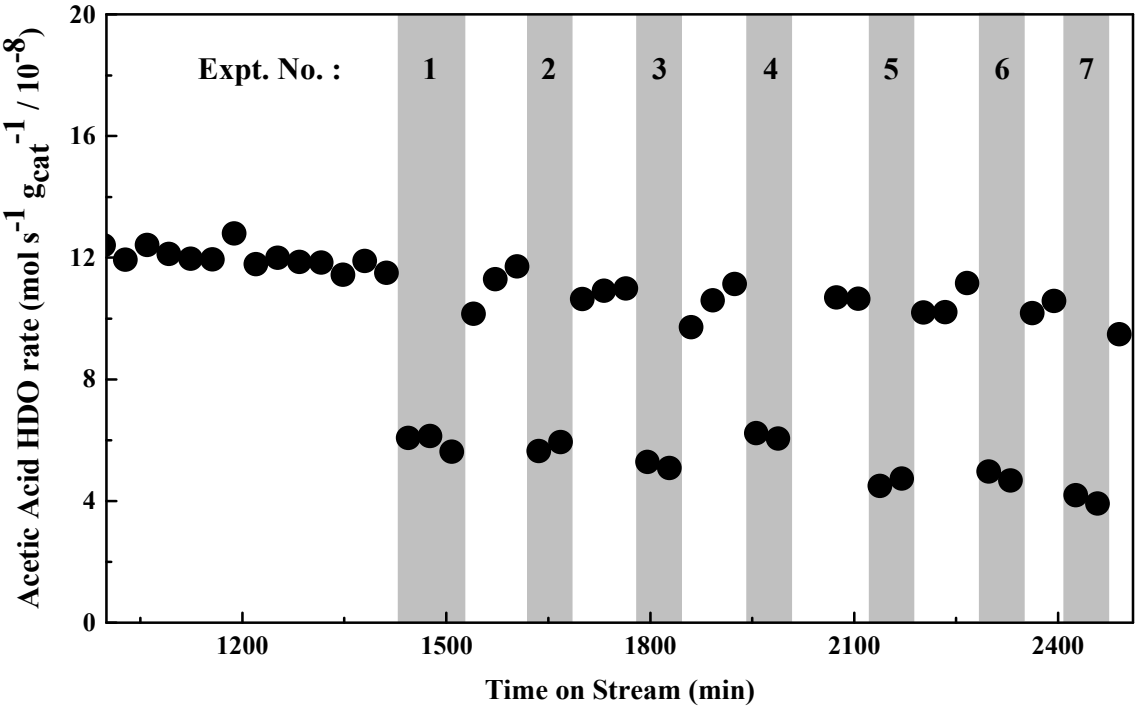

Figure 7. Acetic acid HDO rate vs. time-on-stream during the course of in-situ 2,2-dimethylpropanoic acid (DMPA) titration. The catalyst (~180 mg) was stabilized for ~1450 minutes before in-situ DMPA titration. Shaded areas indicate DMPA/Ar mixtures (0.04 – 0.38 kPa DMPA/ 3.70 kPa argon) were co-fed into the reactant feed comprising 0.50 kPa acetic acid/ balance H_2 with a total flow rate ~ 1.67 cm^3 s^{-1} at reaction temperature = 403 K under ambient pressure. Acetic acid conversion was 5.8 % at steady state in absence of DMPA co-feed.

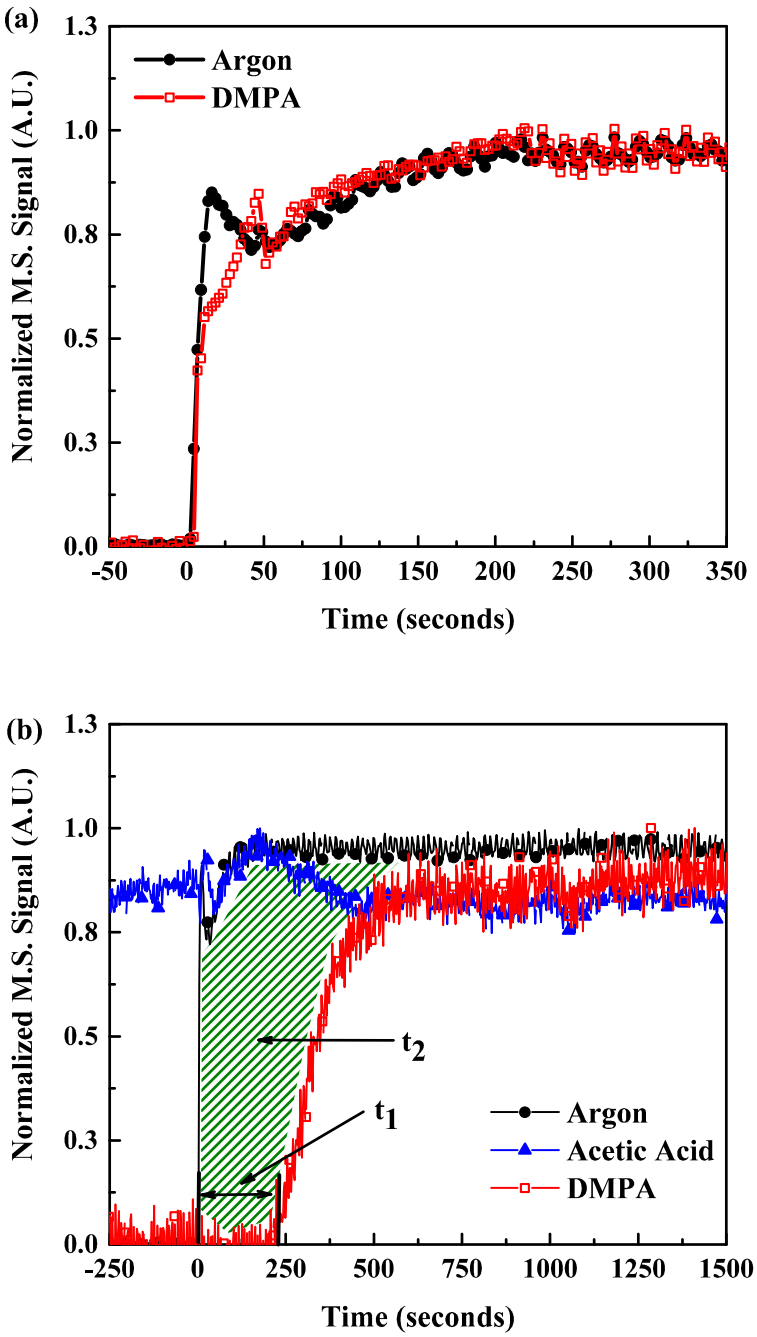

Figure 8. Normalized Ar (m/z = 40), DMPA (m/z =57) and acetic acid (m/z = 43) mass spectrometer signals through (a) a blank reactor and (b) Mo_2C catalyst, during the course of in-situ DMPA titration. The breakthrough time of DMPA and average residence time of DMPA determined by integration of the normalized Ar and DMPA breakthrough curves (green shaded

area) are represented by t_1 and t_2. DMPA/Ar was co-fed as a titrant/ inert tracer with a flow rate of ~ 1.8 x 10^{-5} cm^3 s^{-1}/~0.06 cm^3 s^{-1} into a reactant feed comprising acetic acid/H_2 ~0.50 kPa/balance (total flow rate ~1.67 cm^3 s^{-1}) at a reaction temperature = 403 K under ambient pressure; Mo_2C loading ~180 mg. Acetic acid HDO rates in the presence/absence of DMPA were tracked using GC before 0 s and after 1800 s.

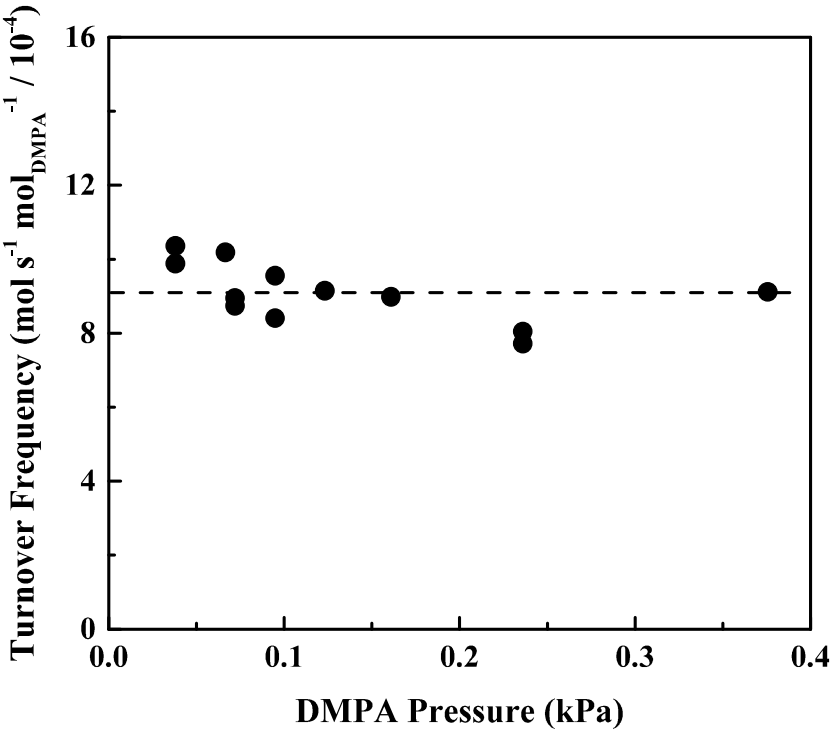

Figure 9. Turnover frequency (TOF) of acetic acid HDO, determined by in-situ DMPA titration, as a function of DMPA pressure (varied from 0.04 – 0.38 kPa). Reaction conditions: temperature = 403 K under ambient pressure; feed composition: acetic acid/H_2 = 0.51 kPa/balance; Mo_2C loading ~180 mg. The amount of DMPA adsorbed was calculated using the breakthrough time, t_1, as shown in Figure 8(b). Acetic acid conversion ranged from ~ 5.0 – 7.0 % at steady state in absence of DMPA co-feed.

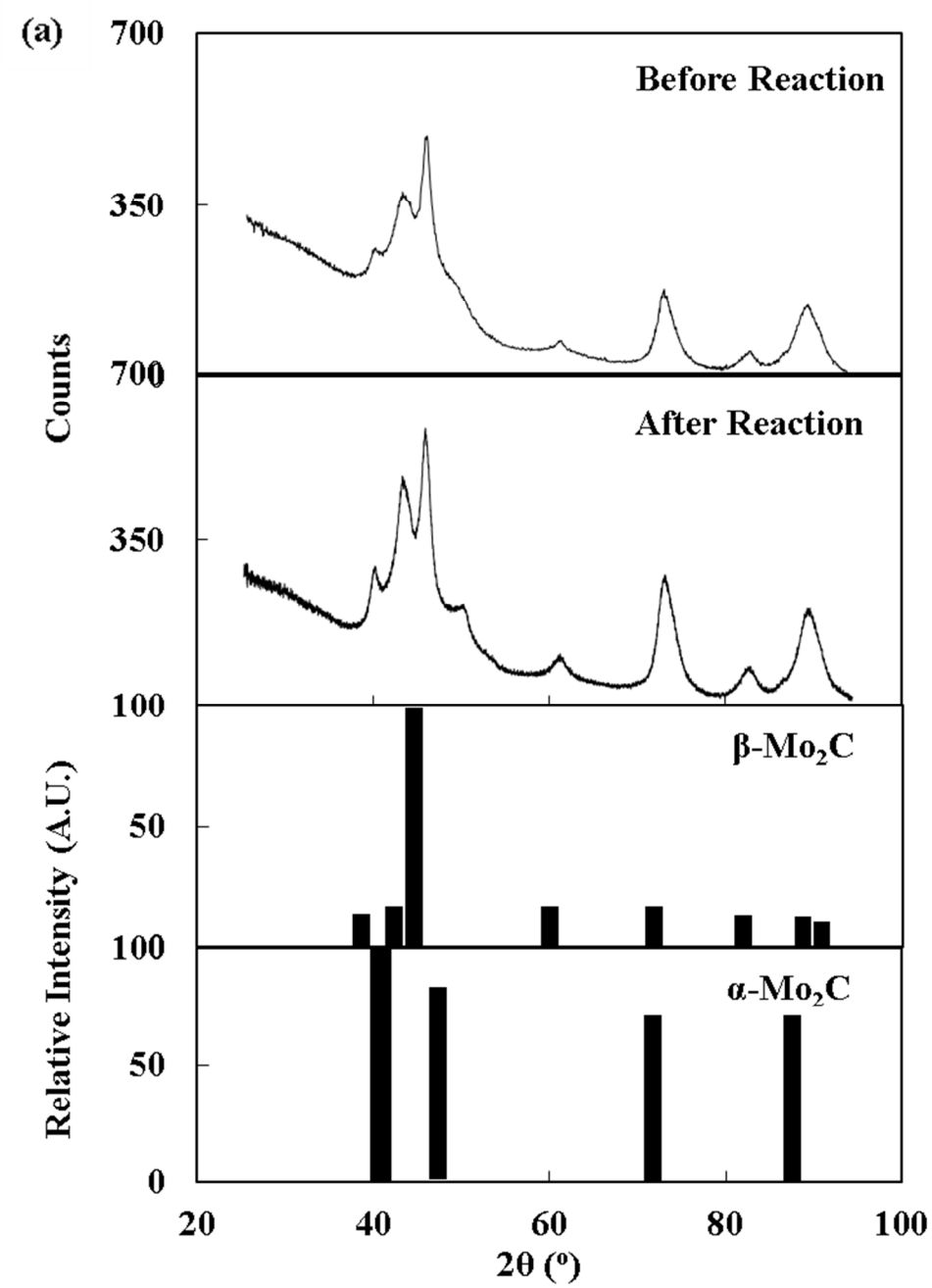
(a)
Before Reaction
After Reaction
β-Mo2C
α-Mo2C
Counts
Relative Intensity (A.U.)
2θ (°)
700
350
700
350
100
50
100
50
0
20
40
60
80
100

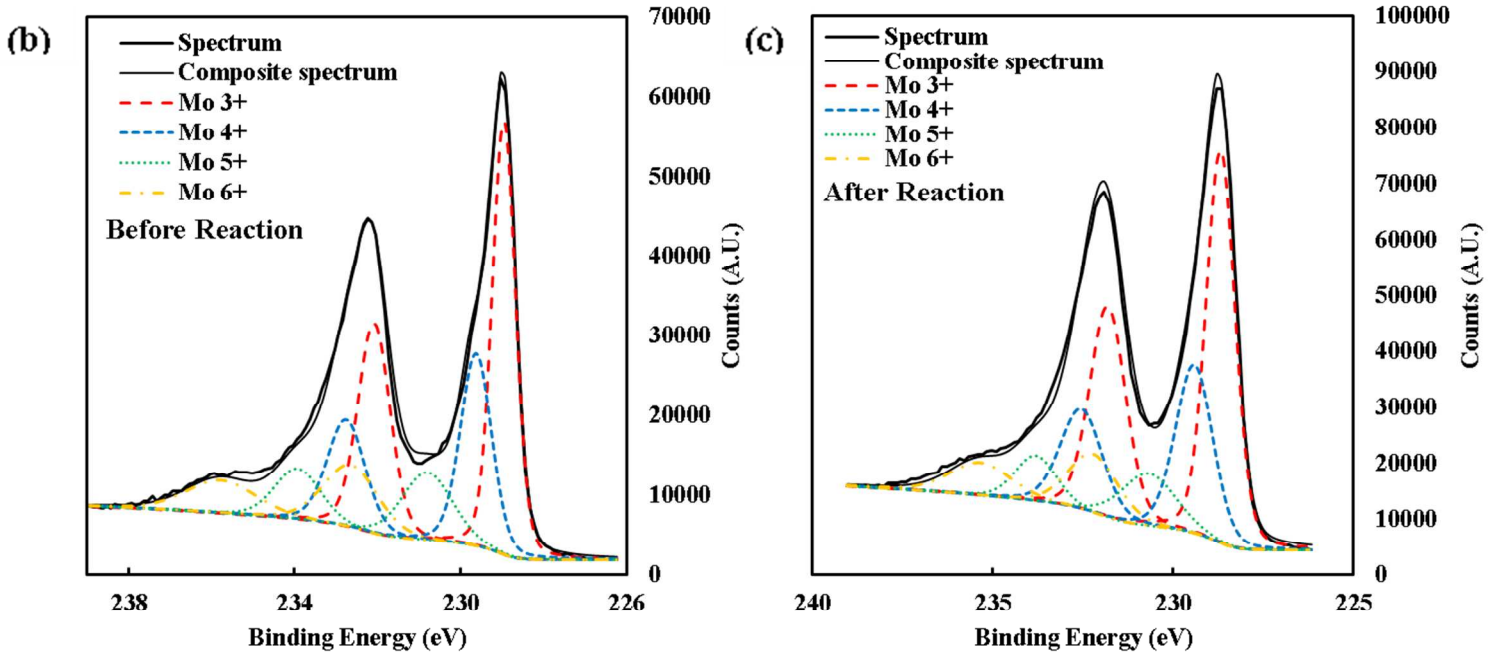

Figure 10. (a) X-ray diffraction patterns of Mo_2C catalysts before and after acetic acid HDO reaction (30 h time- on-stream), including reference diffraction patterns for FCC α-Mo_2C (JCPDS PDF # 00-015-0457) and orthorhombic β-Mo_2C (JCPDS PDF # 01-072-1683). (b) X-ray photoelectron spectrum (XPS) of Mo 3d region of Mo_2C catalysts (b) before and (c) after acetic acid HDO reaction.

Table 1. Experimental conditions and measured kinetics for in-situ DMPA titration of Mo_2C catalysts with catalyst loading ~180 mg for vapor phase acetic acid HDO as shown in Figures 8, 9, and 10.

Expt. No.	DMPA pressure (kPa)	t_1 (s)[a]	t_2 (s)[b]	DMPA flow rate (/ 10^{-6} mol min^{-1})	DMPA adsorbed from t_1 (/ 10^{-5} moles)[c]	DMPA adsorbed from t_2 (/ 10^{-5} moles)[d]	Acetic acid HDO rate before DMPA (/ 10^{-7} mol s^{-1} g_{cat}^{-1})[e]	Acetic acid HDO rate after DMPA (/ 10^{-8} mol s^{-1} g_{cat}^{-1})[e]	Change in Acetic acid HDO rate (/ 10^{-8} mol s^{-1} g_{cat}^{-1})[e]	Turnover frequency from t_1 (/ 10^{-4} mol mol_{DMPA}^{-1} s^{-1})[f]	Turnover frequency from t_2 (/ 10^{-4} mol mol_{DMPA}^{-1} s^{-1})[g]	DMPA product rate (/ 10^{-9} mol s^{-1} g_{cat}^{-1})[h]	DMPA product formed using t_1 (/ 10^{-7} moles)[i]	DMPA product (% of DMPA adsorbed)[j]
1	0.09	198	208	3.8	1.2	1.3	1.2	5.9	5.8	8.4	8.0	7.1	2.5	2.02
2	0.07	238	230	2.6	1.0	1.0	1.2	5.8	5.9	10.2	10.5	5.6	2.4	2.29
3	0.12	140	176	4.9	1.1	1.4	1.1	5.2	5.8	9.1	7.3	6.9	1.7	1.52
4	0.04	345	550	1.5	0.9	1.4	1.1	6.1	5.0	10.4	6.5	4.8	3.0	3.43
5	0.24	86	82	9.5	1.4	1.3	1.1	4.6	6.1	8.0	8.5	7.7	1.2	0.88
6	0.16	119	123	6.4	1.3	1.3	1.1	4.8	6.3	9.0	8.7	7.2	1.5	1.21
7	0.38	51	51	15.1	1.3	1.3	1.1	4.0	6.5	9.1	9.2	9.0	0.8	0.65
8	0.09	137	149	3.8	0.9	0.9	0.9	4.9	4.6	9.6	8.8	6.0	1.5	1.73
9	0.04	245	271	1.5	0.6	0.7	1.0	6.3	3.4	9.9	8.9	4.8	2.1	3.41
10	0.24	86	80	9.5	1.4	1.3	1.0	4.4	5.8	7.7	8.3	0.1	0.0	0.01
11	0.07	254	433	2.8	1.2	2.0	1.2	5.9	5.7	8.7	5.1	4.4	2.0	1.70
12	0.07	224	353	2.8	1.1	1.7	1.1	5.7	5.2	9.0	6.3	4.3	1.7	1.66

[a] the DMPA breakthrough time in seconds (t_1 as shown in Figure 9(b)). [b] the average residence time of DMPA obtained by integrating the area between normalized Ar and DMPA signals as shown in Figure 9(b). [c] obtained by multiplying DMPA molar flow rate by DMPA breakthrough time, t_1. [d] obtained by multiplying DMPA molar flow rate by average DMPA residence time, t_2. [e] Reaction conditions: acetic acid/H_2 ~0.51 kPa/balance with total flow rate ~1.67 cm^3 s^{-1} at reaction temperature = 403 K under ambient pressure, acetic acid conversion (at steady state in the absence of DMPA) during the course of titration were 5.85 %. [f] obtained by ((acetic acid HDO rates without DMPA) − (acetic acid HDO rates with DMPA))/(apparent amount of DMPA adsorbed on the catalysts during DMPA titration from breakthrough time t_1). [g] obtained using the average DMPA residence time t_2. [h] obtained during DMPA co-feed from GC data. [i] obtained by multiplying DMPA product rate by DMPA breakthrough time t_1. [j] obtained by ((DMPA product formed using t_1)x100/(DMPA adsorbed from t_1)).

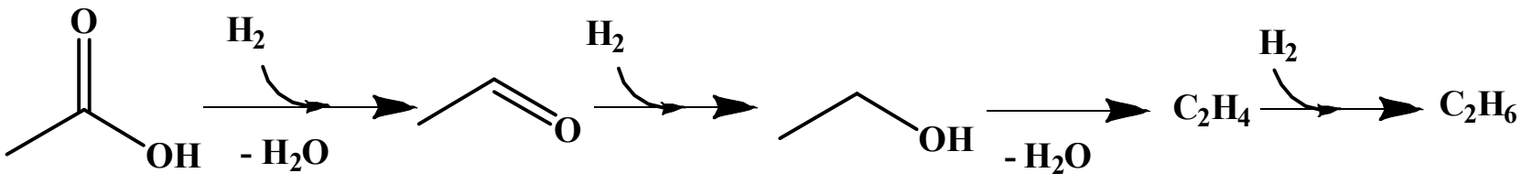

Scheme 1. Proposed acetic acid HDO reaction pathway on Mo_2C catalysts

Scheme 1

$R = CH_3$

$$H_2 + 2\,S_1 \xleftrightarrow{K_1} 2\,H\text{-}S_1 \quad (1)$$

$$RCOOH + S_2 \xleftrightarrow{K_2} RCOOH\text{-}S_2 \quad (2)$$

$$RCOOH\text{-}S_2 + H\text{-}S_1 \xrightarrow{k_3} RC(OH)OH\text{-}S_2 + S_1 \quad (3)$$

$$RC(OH)OH\text{-}S_2 + S_2 \xleftrightarrow{K_4} RCO\text{-}S_2 + H_2O\text{-}S_2 \quad (4)$$

$$RCO\text{-}S_2 + H\text{-}S_1 \xleftrightarrow{K_5} RCHO\text{-}S_2 + S_1 \quad (5)$$

$$H_2O\text{-}S_2 \xleftrightarrow{K_6} H_2O + S_2 \quad (6)$$

$$RCHO\text{-}S_2 \xleftrightarrow{K_7} RCHO + S_1 \quad (7)$$

$$RCOOH + H_2 \longrightarrow RCHO + H_2O$$

Scheme 2

$$H_2 + 2\,S_1 \xleftrightarrow{K_1} 2\,H\text{-}S_1 \quad (1)$$

$$RCOOH + S_2 \xleftrightarrow{K_2} RCOOH\text{-}S_2 \quad (2)$$

$$RCOOH\text{-}S_2 + S_2 \xleftrightarrow{K_3} RCO\text{-}S_2 + HO\text{-}S_2 \quad (3)$$

$$RCO\text{-}S_2 + H\text{-}S_1 \xrightarrow{k_4} RCHO\text{-}S_2 + S_1 \quad (4)$$

$$RCHO\text{-}S_2 \xleftrightarrow{K_5} RCHO + S_2 \quad (5)$$

$$HO\text{-}S_2 + H\text{-}S_1 \xleftrightarrow{K_6} H_2O\text{-}S_2 + S_1 \quad (6)$$

$$H_2O\text{-}S_2 \xleftrightarrow{K_7} H_2O + S_2 \quad (7)$$

$$RCOOH + H_2 \longrightarrow RCHO + H_2O$$

Scheme 2. Proposed reaction schemes for acetic acid deoxygenation to acetaldehyde on Mo_2C catalysts

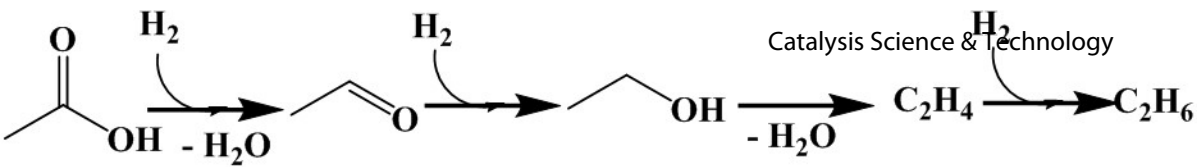
O
OH
H_2
- H_2O
O
OH
C_2H_4
C_2H_6

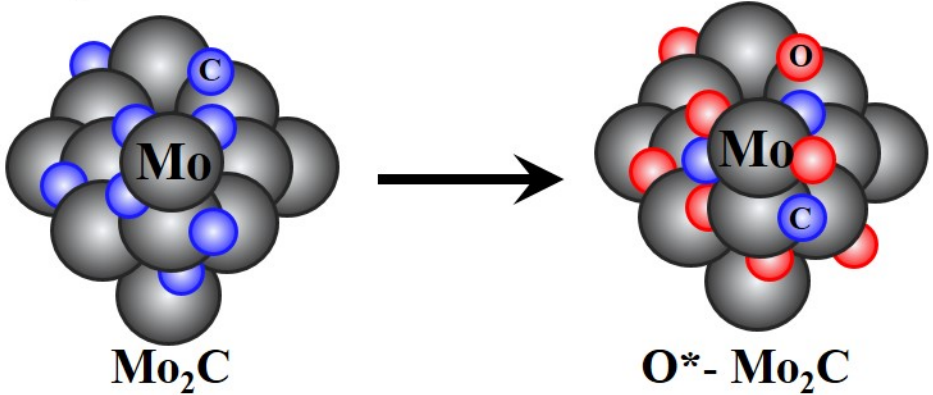
C
Mo
O
Mo
C
Mo_2C
O*- Mo_2C

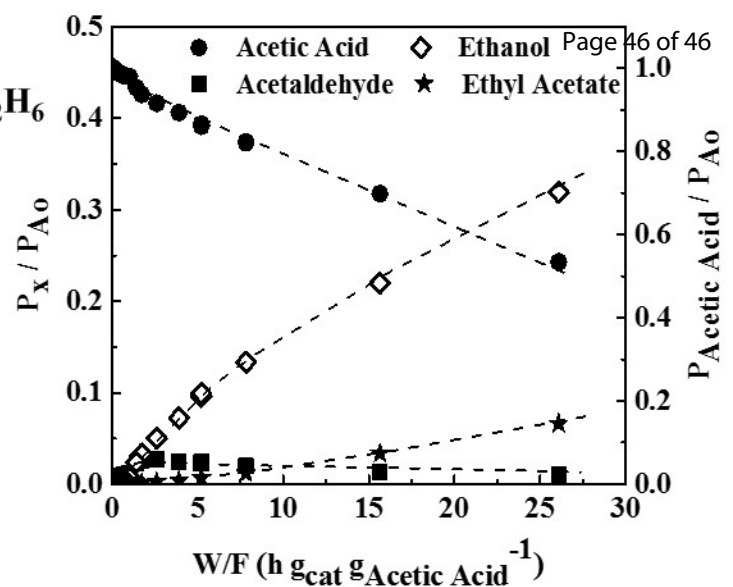
Acetic Acid
Ethanol
Acetaldehyde
Ethyl Acetate
P_X / P_{Ao}
$P_{Acetic\ Acid} / P_{Ao}$
W/F (h g_{cat} $g_{Acetic\ Acid}^{-1}$)
0.0
0.1
0.2
0.3
0.4
0.5
0.0
0.2
0.4
0.6
0.8
1.0
0
5
10
15
20
25
30